Scholars' Mine

Masters Theses   Student Theses and Dissertations

1970

Dynamic analysis of a torsional vibration actuator

Narayandas Trikamdas Ashar

Follow this and additional works at: https://scholarsmine.mst.edu/masters_theses

Part of the Mechanical Engineering Commons

Department:

DYNAMIC ANALYSIS OF A TORSIONAL VIBRATION ACTUATOR

BY

NARAYANDAS TRIKAMDAS ASHAR, 1942-

A

THESIS

submitted to the faculty of

UNIVERSITY OF MISSOURI - ROLLA

in partial fulfillment of the requirements for the

Degree of

MASTER OF SCIENCE IN MECHANICAL ENGINEERING

Rolla, Missouri

1970

Approved by

R. D. Roche   (advisor)   _Richard T. Johnson_

J. Earl Foster

ABSTRACT

The objective of this study is the evaluation of
a mechanical system, which includes a Hooke's joint, as
a possible torsional vibration actuator. The essential
requirement of such a system is to produce a periodically
varying angular motion superimposed upon a mean constant
speed rotation. The basic kinematics of a Hooke's joint
suggest that it could be used to generate the type of
motion desired.

The mechanical arrangement of a system incorporating
a Hooke's joint is described and the governing differen-
tial equations are developed. These equations are simul-
taneous, differential equations of second order and are
highly nonlinear. Values of typical system parameters are
selected and the equations are solved numerically using a
fourth order Runge-Kutta digital solution. The equations
are solved with variations of constants to evaluate the
effect of change in parameters upon the system response.

The numerical results show that the vibration ampli-
tude at the specimen is directly proportional to the motor
speed and the Hooke's joint angle. The frequency of the
vibration at the specimen increases with an increase in
the motor speed but is independent of the Hooke's joint

angle. Increasing the flywheel inertia decreases the variation in the flywheel angular velocity and maintains an output angular velocity which is nearly sinusoidal and closely approximates a second harmonic of the mean flywheel angular velocity.

ACKNOWLEDGEMENT

The author is grateful to Dr. Richard D. Rocke for the suggestion of the topic and for his encouragement, direction and valuable assistance throughout the course of this thesis.

The author is thankful to Dr. Richard T. Johnson for his valuable suggestions.

Thanks are also extended to Mrs. Terry Albrecht and Mrs. Connie Hendrix for neat and speedy typing.

TABLE OF CONTENTS

TABLE OF CONTENTS (Continued)

LIST OF ILLUSTRATIONS

LIST OF TABLES

NOMENCLATURE

D	Diameter of the specimen disc
d	Diameter of the specimen shaft
f	Frequency of the exciting force
f_1	Approximate first natural frequency of torsional vibrations of the specimen
f_n	Natural frequency of the undamped vibrations
I_F	Mass moment of inertia of the flywheel
I_f	Field current
I_{HO}	Mass moment of inertia of the output side of the Hooke's joint
I_M	Mass moment of inertia of the motor
I_{SP}	Mass moment of inertia of the specimen disc
K	Torsional stiffness of the specimen shaft
M	Moment
n	Speed reduction ratio
T	Torque
T_2	Torque at the driver shaft
T_3	Output torque at the driven shaft
T_C	Torque exerted at the coupling
T_{GF}	Torque exerted at the flywheel shaft gear
T_{GM}	Torque exerted at the motor shaft gear
T_{HI}	Torque exerted at the input end of the Hooke's joint
T_M	Torque developed by the motor
t	Thickness of the specimen disc

NOMENCLATURE   (Continued)

β Angle between the driver shaft and the driven shaft of the Hooke's joint

θ Angular position of the driver shaft

θ_1 Angular position of the motor shaft

θ_2 Angular position of the flywheel shaft

θ_3 Angular position of the driven shaft coupling

θ_4 Angular position of the specimen disc

$\emptyset$ Angular position of the driven shaft

ω Circular frequency of the exciting force

ω_2 Angular velocity of the driver shaft

ω_3 Angular velocity of the driven shaft

ω_n Natural frequency of the undamped vibrations

$\cdot$ Time derivative, d/dt

CHAPTER I

INTRODUCTION

During the last twenty-five years or so, adequate knowledge of vibratory phenomena has become an essential requirement for progress in mechanical engineering design. In many system applications involving reciprocating and rotating components subject to internal and external pulsations, vibration control enables performance to be improved without sacrifice of reliability. This is often the key to survival in a highly competitive market.

Costly experience has shown, for example, that engine crankshaft systems are apt to be particularly responsive to torsional excitations as significant resonant conditions may occur within or close to the operating speed ranges. Also, investigation into the torsional vibration characteristics of shaft systems transmitting pulsating torques has become an important part of the design engineer's responsibility. Indeed, satisfactory operation of high-duty transmission systems may be said to depend to a large extent on successful handling of the vibration problems.

Although extensive work has been done in the analytical field of linear torsional vibrations, few devices that simulate the conditions causing torsional vibrations have been made. It is desirable that the models representing

the parts such as crankshafts, gear trains, etc. be tested on a device which duplicates a realistic environment. With such testing, torsional vibration characteristics can be thoroughly investigated to include nonlinear effects.

Kinematics of the Hooke's joint has been known [1] for some time. Hagenbook and Holstein [2] have described the vectorial method by which the bearing loads and the torque for any Hooke's joint may be calculated. Rosenberg [3] has examined the effect of the angularity of the Hooke's joint on the bending stability of the rotating shafts.

From these studies, it is found that the Hooke's joint can be used to generate the type of motion which would be desirable in a torsional vibration testing machine. The purpose of this thesis is to investigate the parameters for a torsional vibration actuator incorporating a Hooke's joint. The governing equations of motion for the system are derived. These equations are nonlinear and have been solved under varied conditions to investigate the dynamic response of a feasible system.

A.   Contents of Thesis

Chapter II summarizes the preliminary investigations made into using a Hooke's joint for a possible torsional vibration actuator. The kinematic relationships for a

single Hooke's joint have been established and the type of motion generated by it is studied to check the suitability of its use in a torsional vibration actuator.

In Chapter III, the description of a mechanical system incorporating a Hooke's joint is given. The differential equations governing the motion of the system have been established after making some simplifying assumptions. Sizes of various components have been selected from which various constants for the equations of motion are determined.

In Chapter IV, the numerical method used in solving the equations of motion is described. A digital computer has been used to obtain the numerical solutions to the governing nonlinear differential equations using a fourth order Runge-Kutta method. In the absence of analytical results, the equations have been solved under the varied conditions and the results compared. The numerical results are also compared with the physical behavior expected of this type of system.

CHAPTER II

PRELIMINARY INVESTIGATIONS

Many power trains in machines utilize a constant
speed motion. With such a motion, if another motion can
be superimposed which is periodic in nature, a source may
be created whose output represents a mean constant speed
plus a small periodic variation. It is desirable that the
periodic variations be sinusoidal and controllable. Such
a source may then be utilized as a torsional vibration
actuator. A study of the kinematic relationship of the
Hooke's joint indicates that the driven shaft of the
Hooke's joint generates the type of motion sought for an
actuator when the driver shaft rotates at a constant speed.
Also, the frequency and the amplitude of variations in the
driven shaft speed can be easily controlled. Hence, further
investigations into the kinematics of the Hooke's joint were
made.

A.   Hooke's Joint

As is well known, a Hooke's joint is not a "constant-
velocity" device. A single Hooke's joint that connects two
non-parallel shafts will produce a periodic non-uniform
output velocity even though the input velocity is constant.
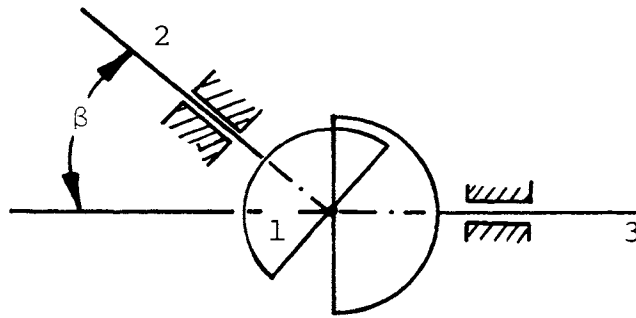
Fig. 2.1   Hooke's Joint

A sketch of a Hooke's joint is given in Fig. 2.1.
In this figure, link 2 is the driver shaft and link 3
is the driven shaft. Link 1 is the cross piece that
connects the two yokes. It can be shown [3] that,
although both shafts must complete one revolution in
the same length of time, the angular velocity ratio of
the two shafts is not constant during a revolution.
Expressed more precisely, the angular velocity ω_3 of the
driven shaft is not at every instant equal to the angular
velocity ω_2 of the driver shaft. In fact, these two
quantities are related by an expression of the type:

$$\frac{\omega_3}{\omega_2} = f(\beta, t)$$

where β is the angle between two shafts.

If angular velocity ω_2 is a constant, the function
$f(\beta, t)$ is a periodic function of time, approximately
sinusoidal and tends to unity as β approaches zero. Hence,

the Hooke's joint could be used to generate the type of motion sought in this study.

B. Kinematic Relations

The kinematic relationship for motion through a single Hooke's joint is expressed in the following formula [2]:

$$\tan \emptyset = \tan \theta \cos \beta \qquad (2.1)$$

where:

θ = Angular displacement of the driver shaft

∅ = Angular displacement of the driven shaft

β = Included angle between the shafts.

Differentiating Eq. (2.1) with respect to time, holding β constant and simplifying, gives:

$$\frac{d\emptyset}{dt} = \left[\frac{\cos \beta}{1-\sin^2\beta\sin^2\theta}\right]\frac{d\theta}{dt} \text{ , or} \qquad (2.2)$$

$$\frac{\omega_3}{\omega_2} = \frac{\cos \beta}{1-\sin^2\beta\sin^2\theta} \qquad (2.3)$$

where $\omega_2 = \frac{d\theta}{dt}$ and $\omega_3 = \frac{d\emptyset}{dt}$.

In Fig. 2.2, ω_3/ω_2 is plotted as a function of angle θ for two values of β. It can be noted from Fig. 2.2 that, for constant ω_2 the variation in the driven shaft velocity ω_3 is periodic in nature, approximately sinusoidal with two
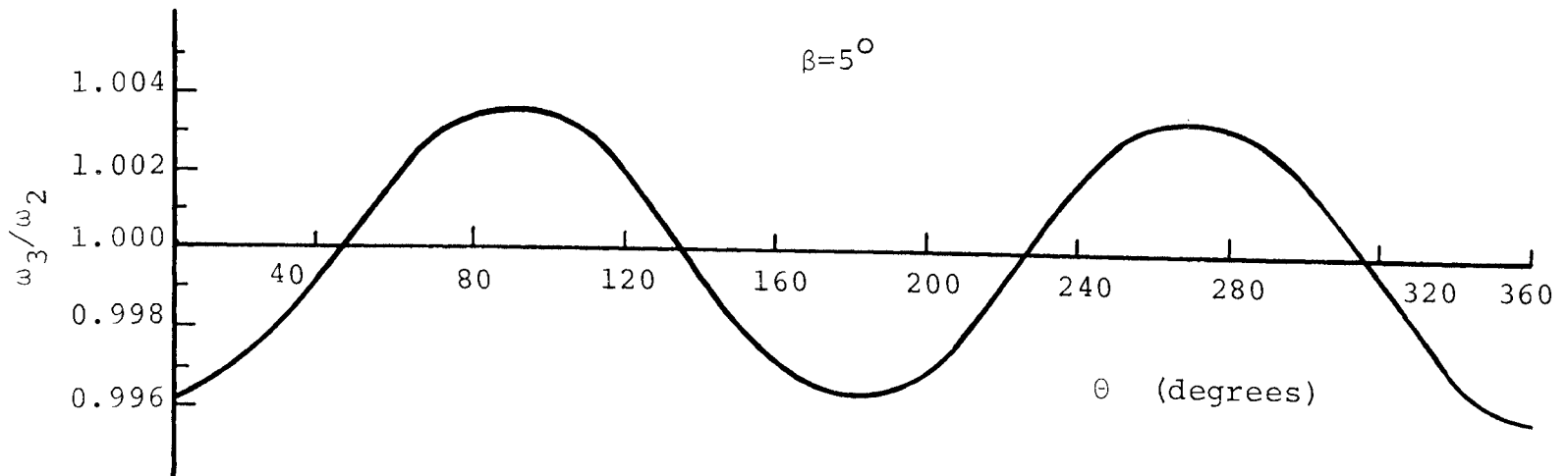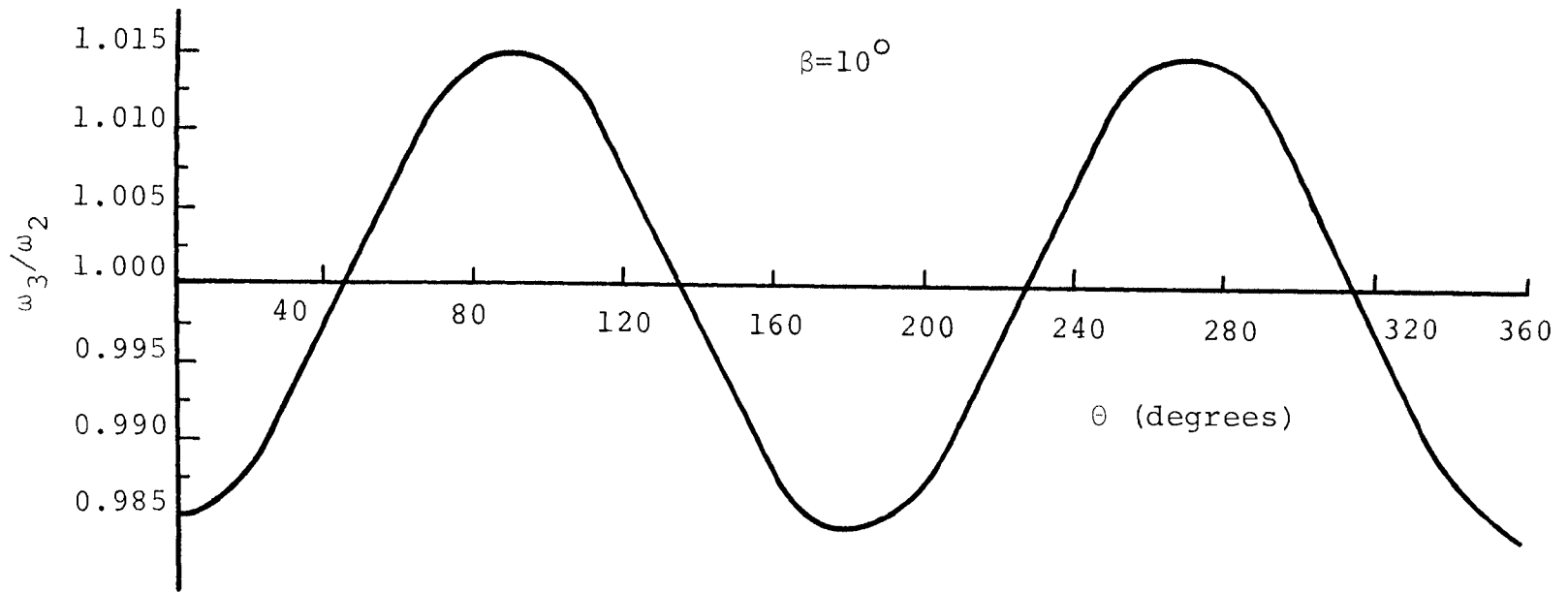
Fig. 2.2 ANGULAR VELOCITY, ω_3/ω_2

cylic changes for one complete revolution of the driver shaft. In other words, the frequency of variation of ω_3 is nearly a second harmonic of ω_2. Also, the ordinates at $\theta(90)$ and $\theta(180)$ are not exactly equal, indicating a departure from pure sinusoidal motion. The values of the ordinates at these points have been tabulated for various values of β and the percentage error has been found, which is defined as:

$$\% \text{ Error} = \frac{\text{Ordinate at } \theta(90) - \text{Ordinate at } \theta(180)}{\text{Average Ordinate}} \times 100.$$

The values of this error measurement are given for a range of β values in Table I.

From Table I it is evident that the angle β must be limited to a certain maximum value if the output velocity is required to be symmetric within a reasonable engineering type accuracy, e.g., limiting β to $\leq 25^\circ$ keeps the error level below ten percent.

Assuming the internal workings of the joint to be conservative, i.e., no energy lost, the input power is equal to the output power, or

$$T_3\omega_3 = T_2\omega_2 \tag{2.4}$$

where:

T_2 = Input torque at the driver shaft

T_3 = Output torque at the driven shaft.

TABLE I

PERCENTAGE ERROR OF ω_3/ω_2

β (degrees)	Ordinate at		Difference in Ordinates	% Error
	$\theta = 90^\circ$	$\theta = 180^\circ$		
0	0	0	0	0
5	0.00382	0.00381	0.00001	0.26
10	0.01543	0.01519	0.00024	1.60
15	0.03528	0.03407	0.00121	3.45
20	0.06418	0.06031	0.00387	6.0
25	0.10338	0.09369	0.00969	9.4
30	0.15470	0.13397	0.02073	13.4
35	0.22077	0.18085	0.03992	18.4
40	0.30541	0.23396	0.07145	23.4
45	0.41421	0.29289	0.12132	29.3

Substituting for ω_3/ω_2 from Eq. (2.3) into Eq. (2.4) gives:

$$T_3 = \left[\frac{1-\sin^2\beta\sin^2\theta}{\cos\beta} \right] T_2 . \qquad (2.5)$$

If the driver shaft is rotating at a constant velocity, the input torque T_2 will be constant for constant power; hence, output torque T_3 will not be constant. In fact, it will undergo cyclic changes similar to that of the driven shaft velocity ω_3.

Differentiating Eq. (2.2) with respect to time and simplifying, an expression for the output shaft acceleration $\dot{\omega}_3$ is obtained, which is:

$$\dot{\omega}_3 = \frac{d^2\phi}{dt^2} = \left[\frac{\cos\beta\sin^2\beta\sin(2\theta)}{(1-\sin^2\beta\sin^2\theta)^2} \right] (\frac{d\theta}{dt})^2 , \text{ or}$$

$$\frac{\dot{\omega}_3}{\omega_2^2} = \frac{\cos\beta\sin^2\beta\sin(2\theta)}{(1-\sin^2\beta\sin^2\theta)^2} . \qquad (2.6)$$

Note that $\frac{d\theta}{dt} = \omega_2$ is taken to be a constant, i.e., only a constant angular velocity is considered. Figure 2.3 shows a plot of angular acceleration $\dot{\omega}_3$ as a function of θ for various values of β. In this figure, the non-dimensional quantity $\dot{\omega}_3/\omega_2^2$ is plotted.
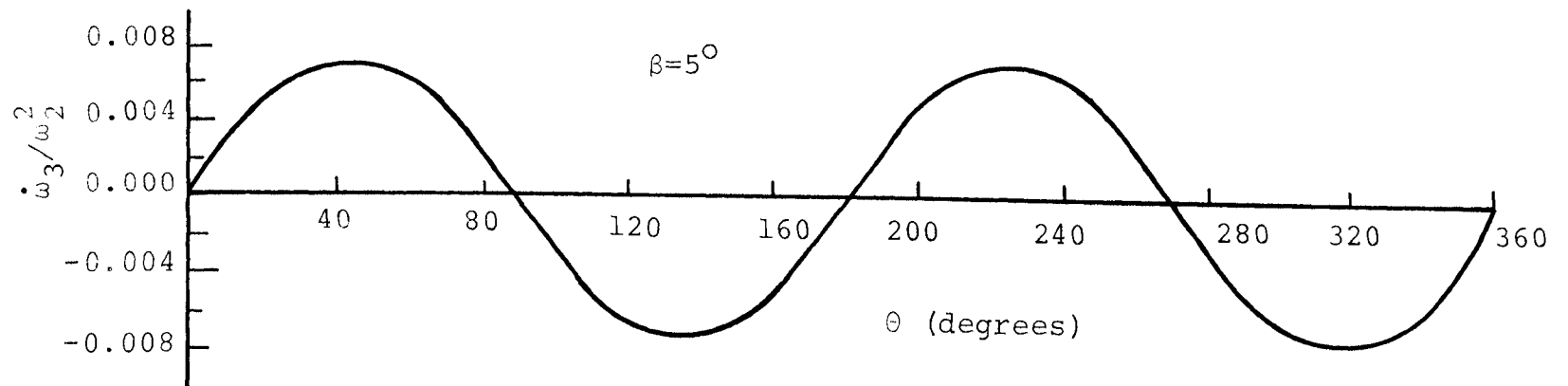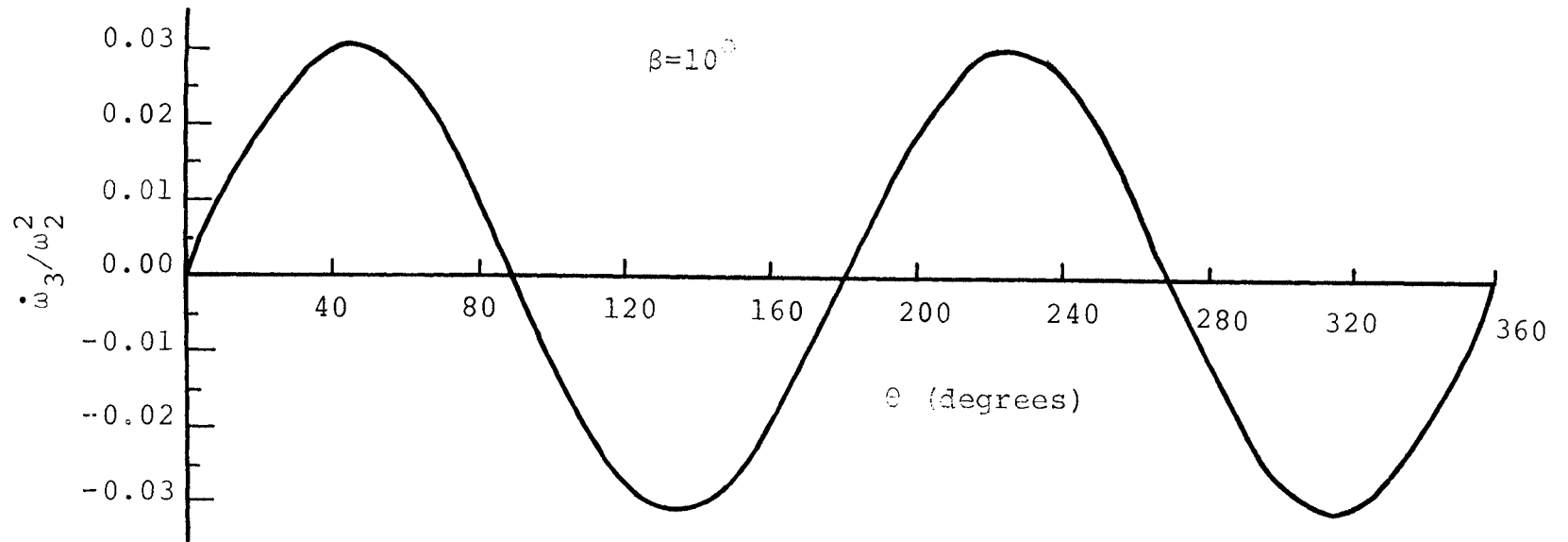
Fig. 2.3 ANGULAR ACCELERATION, $\dot{\omega}_3/\omega_2^2$

It should be noted from the graph that the maximum angular acceleration, for a given ω_2, increases with angle β and is periodic in nature, approximately sinusoidal. Table II gives the values of the ratio of maximum angular acceleration $\dot{\omega}_3$ to ω_2^2 for various values of β.

The maximum angular acceleration times the mass moment of inertia of the driven member gives the maximum value of the pulsating torque created by the inertia of the driven member. The effect of this pulsating torque on the driver shaft will be superimposed upon the torque required for constant power at the driver shaft; hence, variations in the driver shaft velocity may be expected. Also, the value of the maximum pulsating inertia torque of the driven member will have to be taken into account for the design of various components of the actuator. To completely analyze the motion throughout the various parts of the actuator, the differential equations of motion must be defined and solved. This has been com- pleted in Chapter III by applying Newton's second law of motion to the various parts of the total system with the kinematic equations of motion of the Hooke's joint included.

TABLE II

RATIO OF MAXIMUM VALUE OF $\dot{\omega}_3/\omega_2^2$ FOR VARIOUS VALUES OF β

β (degrees)	Ratio	β (degrees)	Ratio
0	0.00000	25	0.19893
5	0.00763	30	0.29373
10	0.03061	35	0.41705
15	0.06927	40	0.57554
20	0.12480	45	0.78384

CHAPTER III

SYSTEM DEFINITION AND EQUATIONS OF MOTION

A.   Mechanical Arrangement

A sketch of a possible torsional vibration actuator design incorporating a single Hooke's joint is shown in Fig. 3.1. A D.C. shunt motor and a flywheel represents the basic power source. The driver shaft of the Hooke's joint is rigidly connected to the flywheel shaft. The driven shaft of the Hooke's joint and the specimen to be tested are mounted on a separate block which is hinged to the main platform at a point directly below the center of the Hooke's joint.

The motor drives the flywheel through a reduction gear having a speed reduction ratio of 3:1. The D.C. shunt motor is a motor which exhibits a good speed regulation characteristic · The speed of the motor can be controlled by varying the field current of the motor through a field rheostat. The speed control of the motor is necessary to change the frequency of excitation to the specimen. The reduction gear is used to reduce the speed of the driver shaft of the Hooke's joint.

It has been shown in Eq. (2.3) that the nature of the driven shaft velocity depends on the characteristics of the driver shaft velocity. If ω_2 is nearly constant,
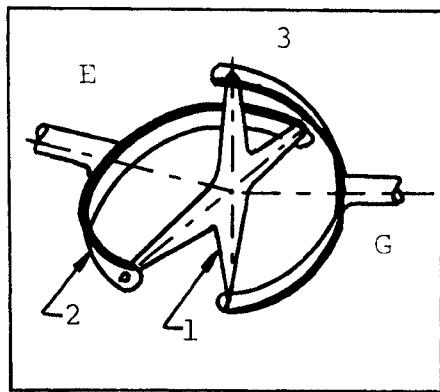
F. Hooke's Joint
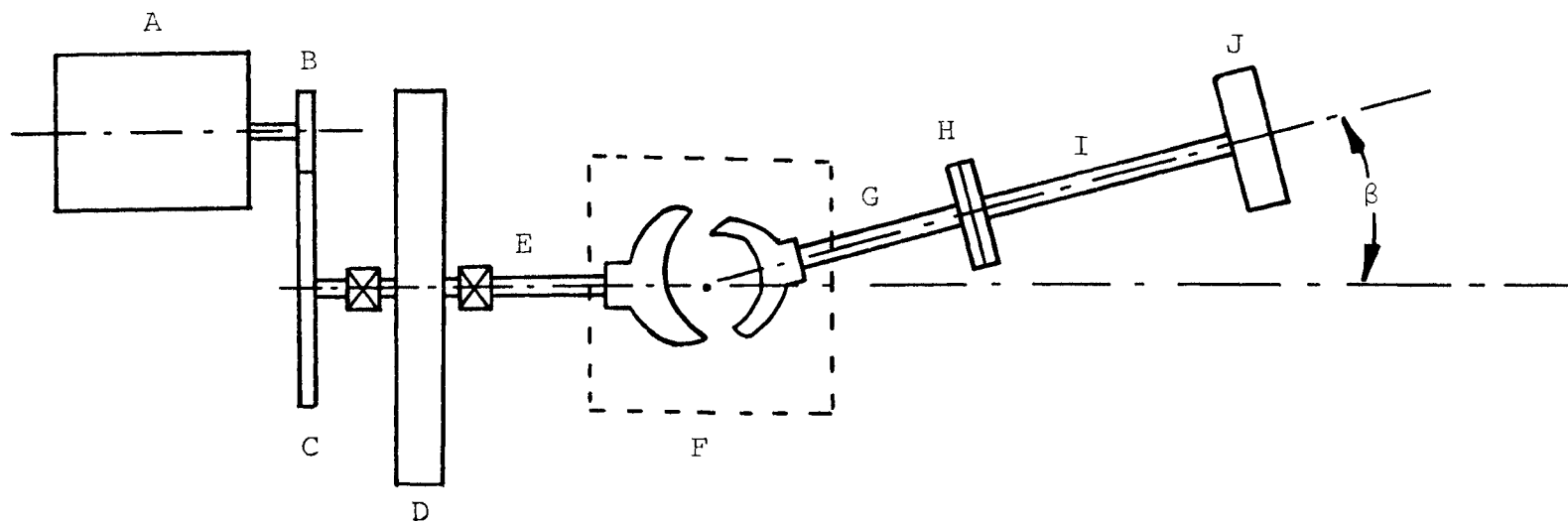
Fig. 3.1   Schematic Sketch of Torsional Vibration Actuator

In Fig. 3.1,

A	Motor	H	Coupling
B	Motor Shaft Gear	I	Specimen Shaft
C	Flywheel Shaft Gear	J	Specimen Disc
D	Flywheel	1	Cross Arm
E	Driver Shaft	2	Driving Yoke
F	Hooke's Joint	3	Driven Yoke
G	Driven Shaft		

the variations in the driven shaft velocity ω_3 are nearly sinusoidal. Because of this, a D.C. shunt motor with good speed regulation is used as the prime mover. Moreover, to reduce the effect of the pulsating inertia torque from the driven side upon the driver side, a flywheel is used. This aids in maintaining a minimal variation in the speed of the driver shaft.

A specimen is connected to the driven shaft by a rigid coupling. The input to the specimen will be nearly a sinusoidal variation which will excite torsional oscillations in the specimen. The angle β between the driver shaft and the driven shaft of the Hooke's joint is considered to be a constant with time. However, it could be changed between tests; thus, providing a change in the amplitude of the input excitation to the specimen.

B. Governing Equations of Motion

B.1 Assumptions

The following assumptions are made in the derivation of the equations of motion:

1. Friction in the bearings and the reduction gear is neglected.

2. All the components of the actuator, except the specimen shaft, are rigid.

3. The specimen shaft is massless and acts as a torsional spring only. Specimen disc is considered to be a rigid inertia.

4. The backlash and the slippage for the entire device are neglected.

5. Angle β between the driver shaft and the driven shaft is considered constant for any given configuration.

6. The torque-speed curve for D.C. shunt-motor is selected from typical manufacturer's data.

B.2 Free Body Diagrams for Components

On the basis of above assumptions, the torsional vibration machine may be subdivided into four major components - motor, flywheel, driven shaft and specimen. A free body diagram for each of these major components is shown and the equations of motion are written by applying Newton's second law of motion.

Motor
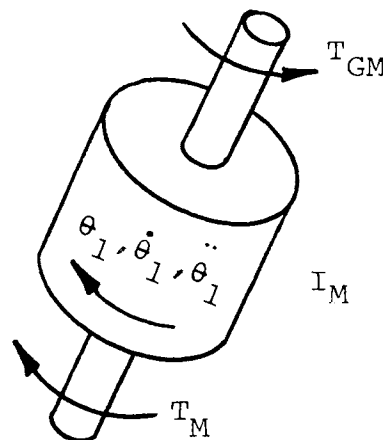
Fig. 3.2 Free Body Diagram for Motor

The free body diagram for the motor is shown in
Fig. 3.2. θ_1, $\dot{\theta}_1$ and $\ddot{\theta}_1$ denote the angular position, the
angular velocity, and the angular acceleration of the
motor shaft, respectively. In the diagram the terms are:

T_M = Torque developed by the motor

T_{GM} = Torque exerted at the motor shaft gear

I_M = Mass moment of inertia of the motor arma-
ture, motor shaft, and the motor shaft gear.

Summing the moments on the motor shaft by applying
$\Sigma M = I\ddot{\theta}$, gives:

$$T_M - T_{GM} = I_M \ddot{\theta}_1 . \qquad (3.1)$$

Flywheel
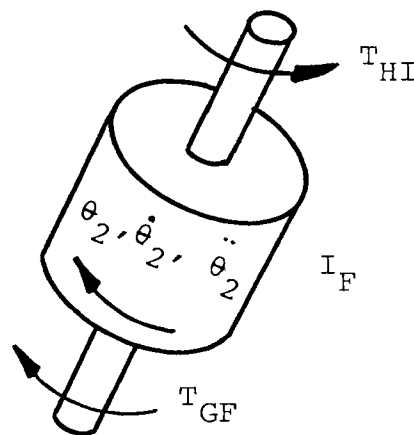
Fig. 3.3 Free Body Diagram for Flywheel

Let θ_2, $\dot{\theta}_2$ and $\ddot{\theta}_2$ denote the angular position, the
angular velocity, and the angular acceleration of the fly-
wheel, respectively. Also,

T_{GF} = Torque exerted at the gear on the flywheel shaft

T_{HI} = Torque at the input end of the Hooke's joint

I_F = Mass moment of inertia of the flywheel, flywheel shaft and the gear on the flywheel shaft.

Applying $\Sigma M = I\ddot{\theta}$ to this free body, gives:

$$T_{GF} - T_{HI} = I_F\ddot{\theta}_2 . \qquad (3.2)$$

Driven Shaft
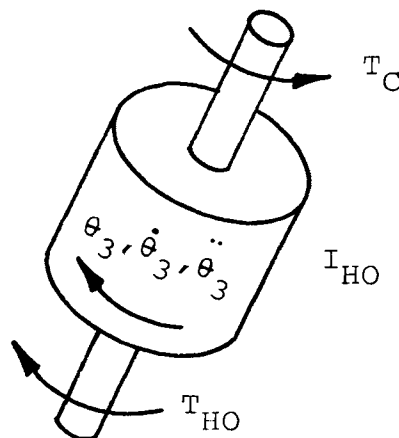
Fig. 3.4 Free Body Diagram for Driven Shaft

Let θ_3, $\dot{\theta}_3$ and $\ddot{\theta}_3$ denote the angular position, the angular velocity, and the angular acceleration of the driven shaft, respectively. Also,

T_{HO} = Torque exerted at the output shaft
(driven shaft)

T_C = Torque at the coupling which connects
the driven shaft to the specimen

I_{HO} = Mass moment of inertia of the output
shaft including the coupling which
connects it to the specimen.

The torque equation for this free body is:

$$T_{HO} - T_C = I_{HO} \, \ddot{\theta}_3 . \qquad\qquad (3.3)$$

Specimen
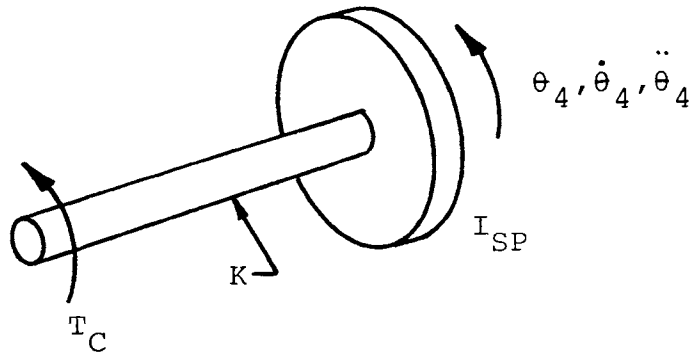
Fig. 3.5   Free Body Diagram for Specimen

The specimen is defined to be a simple model of a
system to be tested.   In Fig. 3.5, θ_4, $\dot{\theta}_4$, and $\ddot{\theta}_4$ denote
the angular position, the angular velocity, and the angular
acceleration of the rigid specimen disc.   The parameters
defining the specimen are:

$$I_{SP} = \text{Mass moment of inertia of the specimen}$$
$$\text{disc}$$

$$K = \text{Torsional stiffness of the specimen shaft.}$$

Because the torque at the either end of the specimen shaft must be equal,

$$T_C = I_{SP}\ddot{\theta}_4$$

$$\therefore\ K(\theta_3-\theta_4) = I_{SP}\ddot{\theta}_4,\ \text{or}$$

$$I_{SP}\ddot{\theta}_4 - K(\theta_3-\theta_4) = 0, \tag{3.4}$$

since $\quad T_C = K(\theta_3-\theta_4).$ $\tag{3.5}$

B.3 System Equations of Motion

The relation between the different torques are found in order to combine the equations of motion for the separate components to get the equations of motion for the whole system. As the backlash and the slippage between the gears are neglected :

$$\theta_2 = n\,\theta_1 \tag{3.6}$$

where n = speed reduction ratio, a number less than unity. Differentiating Eq. (3.6) with respect to time gives:

$$\dot{\theta}_2 = n\,\dot{\theta}_1. \tag{3.7}$$

An additional differentiation of Eq. (3.7) gives:

$$\ddot{\theta}_2 = n\,\ddot{\theta}_1. \tag{3.8}$$

As the frictional losses of the reduction gear are neglected,

$$T_{GM}\,\dot{\theta}_1 = T_{GF}\,\dot{\theta}_2 , \text{ or}$$

$$T_{GM} = \frac{\dot{\theta}_2}{\dot{\theta}_1}\,T_{GF} = n\,T_{GF}. \tag{3.9}$$

Substituting for T_{GM} from Eq. (3.9) and $\ddot{\theta}_1$ from Eq. (3.8) into Eq. (3.1) gives:

$$T_M - n\,T_{GF} = I_M\,\frac{\ddot{\theta}_2}{n} , \text{ or}$$

$$I_M\ddot{\theta}_2 + n^2\,T_{GF} = n\,T_M. \tag{3.10}$$

In Eq. (2.5), the input-output torque relationship was established for a single Hooke's joint. Putting this into the present nomenclature gives:

$$T_{HI} = \left[\frac{\cos\beta}{1-\sin^2\beta\sin^2\theta_2}\right]T_{HO}. \tag{3.11}$$

Substituting for T_{HI} from Eq. (3.11) into Eq. (3.2) gives:

$$T_{GF} - \left[\frac{\cos\beta}{1-\sin^2\beta\sin^2\theta_2}\right]T_{HO} = I_F\ddot{\theta}_2 \tag{3.12}$$

A further substitution for T_{GF} from Eq. (3.12) into Eq. (3.10) gives:

$$(n^2 I_F + I_M) \ddot{\theta}_2 + n^2 T_{HO} \left[\frac{\cos \beta}{1 - \sin^2 \beta \sin^2 \theta_2} \right] = n \, T_M. \tag{3.13}$$

Also, substituting for T_C from Eq. (3.5) into Eq. (3.3) gives:

$$T_{HO} - K(\theta_3 - \theta_4) = I_{HO} \ddot{\theta}_3, \quad \text{or}$$

$$T_{HO} = I_{HO} \ddot{\theta}_3 + K(\theta_3 - \theta_4). \tag{3.14}$$

Putting the result for T_{HO} from Eq. (3.14) into Eq. (3.13) gives:

$$(n^2 I_F + I_M) \ddot{\theta}_2 + n^2 \left[I_{HO} \ddot{\theta}_3 + K(\theta_3 - \theta_4) \right] \left[\frac{\cos \beta}{1 - \sin^2 \beta \sin^2 \theta_2} \right] = n T_M. \tag{3.15}$$

It has already been established for a single Hooke's joint in Eq. (2.1), using the present nomenclature, that

$$\tan \theta_3 = \tan \theta_2 \cos \beta \tag{3.16}$$

Differentiating this expression with respect to time, holding β constant, gives:

$$\dot{\theta}_3 = \left[\frac{\cos \beta}{1 - \sin^2 \beta \sin^2 \theta_2} \right] \dot{\theta}_2.$$

Differentiating this again with respect to time gives:

$$\ddot{\theta}_3 = \left[\frac{\cos\beta}{1-\sin^2\beta\sin^2\theta_2}\right]\ddot{\theta}_2 + \left[\frac{\cos\beta\sin^2\beta\sin(2\theta_2)}{(1-\sin^2\beta\sin^2\theta_2)^2}\right]\dot{\theta}_2^2 \ .$$

(3.17)

Note that $\dot{\theta}_2$, the flywheel angular velocity, is not considered to be constant which may be the case in the transient as well as the steady state condition of the actuator because of the total system dynamics. Substituting for θ_3 and $\ddot{\theta}_3$ from Eq. (3.16) and Eq. (3.17), respectively, into Eq. (3.15) and simplifying, gives:

$$\left\{n^2 I_F + I_M + n^2 I_{HO}\left[\left(\frac{\cos\beta}{1-\sin^2\beta\sin^2\theta_2}\right)^2\right]\right\}\ddot{\theta}_2$$

$$+ \left\{n^2\ I_{HO}\left[\left(\frac{\cos^2\beta\sin^2\beta\sin(2\theta_2)}{(1-\sin^2\beta\sin^2\theta_2)^3}\right)\right]\right\}\dot{\theta}_2^2$$

$$+ \left\{n^2 K\left[\left(\frac{\cos\beta}{1-\sin^2\beta\sin^2\theta_2}\right)\right]\tan^{-1}(\tan\theta_2\cos\beta)\right\}$$

$$- \left\{n^2 K\left[\left(\frac{\cos\beta}{1-\sin^2\beta\sin^2\theta_2}\right)\right]\theta_4\right\} = n\ T_M.$$

(3.18)

This represents one of the equations of motion for the system. Substituting for θ_3 from Eq. (3.16) into Eq. (3.4) gives another equation, which is:

$$I_{SP}\ddot{\theta}_4 + K\theta_4 - K\tan^{-1}(\tan\theta_2\cos\beta) = 0 \qquad (3.19)$$

Equations (3.18) and (3.19) are two simultaneous differential equations governing the motion of the torsional actuator system which includes a simple single degree of freedom model (specimen).

C.   Design of the Major Components

To solve the equations of motion, parameters need to be specified for the major system components. To do this, a typical specimen was first sized such that its fundamental frequency was near 25 cps, which should represent a realistic first mode crankshaft model. The remaining elements, i.e., shafts, couplings, Hooke's joint, and motor were then sized accordingly, assuming all other elements to act as rigid bodies. Upon examination of the first few solutions, it was felt that the changes, if necessary, could be made in the parameters. Primarily, only a change in flywheel inertia was envisioned in order to observe some indication of the system response as a function of flywheel inertia.

Specimen

A specimen which could be used in conjunction with the torsional system is shown in Fig. 3.6. It consists of a solid elastic shaft of diameter d and length l, at one end of which is fixed a rigid circular disc of diameter D and thickness t.
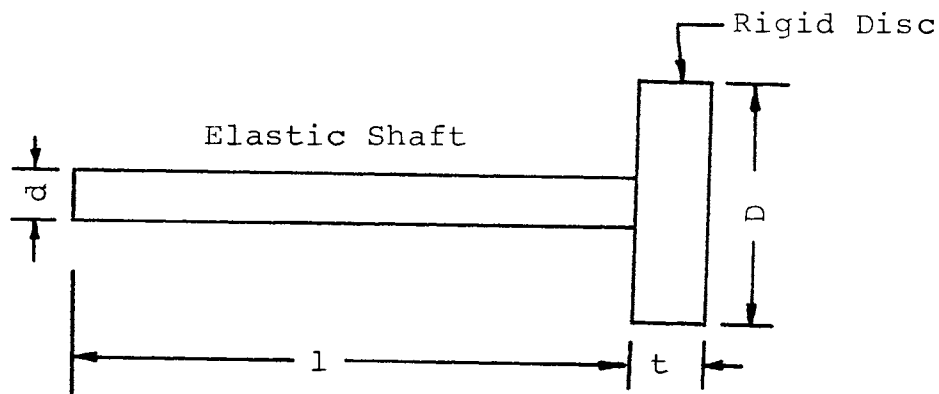
Fig. 3.6   Torsional Specimen

The dimensions of the specimen are so fixed that its lowest natural frequency of torsional vibration is below 25 cps. This corresponds to a motor speed of 2250 rpm. Motors with this speed rating are normally available.

In the derivation of the equations of motion, the specimen shaft was assumed to be a massless elastic element. However, for the calculation of natural frequency of vibration, the specimen shaft is considered to be a continuous system, on one end of which a rigid disc is fixed. The transcendental frequency equation for such a system has been derived and extensive tables made to include the first few natural frequencies for various specimen characteristics [4]. Hence, the above mentioned procedure was adopted in analyzing the specimen as a separate system. The method for finding the natural frequency of torsional vibration of the specimen is outlined in Appendix A. The dimensions of various specimens with the lowest natural frequency below 25 cps are given in Table III.

TABLE III

DIMENSIONS FOR VARIOUS TORSIONAL VIBRATION
SPECIMENS

d (inches)	l (inches)	D (inches)	t (inches)	f_1 (cps)	I_{SP} (lb.in.sec^2)
5/8	15	8	2	23.0	0.628
1/2	15	8	1	20.5	0.314
1/2	12	8	2	16.3	0.628
1/2	12	8	$1^1/_2$	18.8	0.471
1/2	12	8	1	23.0	0.314

Driven Side Coupling

The coupling which connects the driven shaft to the specimen is required to be rigid in comparison to the specimen shaft. A coupling with 4 inch outside diameter and thickness of 1 1/2 inches was selected. The mass moment of inertia of this coupling is 0.027 lb.in.sec^2. Adding approximately ten percent of this to take into account the mass moment of inertia of the driven shaft and the output side of the Hooke's joint gives:

$$I_{HO} = 0.03 \text{ lb.in.sec}^2$$

Flywheel

The flywheel helps in maintaining a constant driver shaft velocity. The larger the flywheel inertia, the smaller will be the variations in the driver shaft velocity. The mass moment of inertia of the flywheel I_F was chosen to be about thirty times the maximum value of mass moment of inertia of the specimen disc, which gives I_F to be 20 lb.in.sec^2. The mass moments of inertia of the flywheel shaft gear, the driver shaft, and the input side of the Hooke's joint are assumed to be included in this value. A general guideline used was to have a flywheel inertia of one or two orders of magnitude greater than the driven side inertia. The system response was found using this value of I_F and then changed, keeping all the other parameters the same, to judge the dependence of the system response on I_F.

Motor

The characteristics of a D.C. shunt motor with a nominal speed of 2000 rpm were used. The motor supplies the power to overcome the friction and the inertia torque exerted by the driven parts of the Hooke's joint. The variations in the acceleration of the driven shaft are assumed to be sinusoidal in sizing the motor. Hence, the variations of the inertia torque are also sinusoidal. When the steady state condition is reached, the motor has to supply the power to accelerate the driven parts from the mean speed to the maximum speed. As the load torque varies sinusoidally, the average value for the load torque is used to compute the approximate horsepower of the motor.

At full load, the motor speed is 1200 rpm which is equivalent to a flywheel speed ω_2 of 42 rad/sec. The angle β has been limited to 15° so that the variations in the angular velocity of the driven shaft are nearly symmetric for constant ω_2. It has been shown in Table II that, for $\beta = 15^{\circ}$:

$$\dot{\omega}_3 \text{ (maximum)} = 0.06927 \ \omega_2{}^2$$

$$\therefore \text{ Maximum acceleration} = 121 \text{ rad/sec}^2.$$

The mass moment of inertia of the driven side consists of the mass moment of inertia of the driver shaft, the coupling, and the specimen disc. The inertia of the specimen shaft, being small in comparison, is neglected.

The maximum mass moment of inertia of the driven side is found to be 0.658 lb.in.sec^2.

$$\text{Max. inertia torque} = \text{Max. acceleration} \times$$
$$\text{Max. mass moment of inertia} =$$
$$121 \times 0.658 = 80 \text{ lb.in.sec}^2.$$

For the sinusoidal variations, the average inertia torque over a half cycle is 0.64 times the maximum inertia torque.

$$\therefore \text{ Average inertia torque} = 0.64 \times 80 = 51 \text{ lb.in.}$$

The speed of the driver side is not constant, hence, the average value is used to compute the horsepower required as given by:

$$\text{h.p.} = \frac{2\Pi NT}{33,000}$$

where:

N = speed in rpm

T = torque in lb.ft.

$$\therefore \text{ h.p.} = \frac{2\Pi \times 400 \times 51/12}{33,000} = 0.325.$$

In order to account for the frictional losses etc., a 1/2 h.p., 2000 rpm, 125 volt D.C. shunt motor was considered as being adequate for the use in the torsional vibration actuator. With the use of the flywheel, the size of the motor could be reduced as the flywheel resists part of the inertia load torque. However, no such reduction

in the horsepower rating of the motor was considered as a
conservative approach was taken.

The mass moment of inertia of the armature of the
motor can be found by considering it as a solid circular
bar. For this size of the motor, the mass moment of
inertia I_M is about 0.025 lb.in.sec^2. The mass moment of
inertia of the motor shaft and the gear on the motor shaft
are assumed to be included in this value.

Total System Parameters

The values of the different parameters of the actuator
as found in this section have been summarized in Table IV.
The first specimen of Table III was selected for analysis,
hence, its relevant values are given in this table.

TABLE IV

VALUES OF ACTUATOR PARAMETERS

Parameter	Description	Value
I_M	Mass moment of inertia of the motor	0.025 lb. in. $\sec^2$
I_F	Mass moment of inertia of the flywheel	20.0 lb. in. $\sec^2$
I_{HO}	Mass moment of inertia of the output side of Hooke's joint	0.03 lb. in. $\sec^2$
I_{SP}	Mass moment of inertia of the disc of the specimen	0.628 lb. in. $\sec^2$
K	Torsional stiffness of the shaft of the specimen	12000 lb. in./rad
n	Speed reduction ratio	0.33

CHAPTER IV

SOLUTIONS AND RESULTS

A.   Solutions of the Equations of Motion

Table IV gives the values of various constants used
to obtain a numerical solution. Substituting these
values into Eq. (3.18) and Eq. (3.19) gives:

$$\left[2.245 + 0.00333 \left(\frac{\cos\beta}{1-\sin^2\beta\sin^2\theta_2} \right)^2 \right] \ddot{\theta}_2$$

$$+ \left[0.00333 \left(\frac{\sin^2\beta\cos^2\beta\sin(2\theta_2)}{(1-\sin^2\beta\sin^2\theta_2)^3} \right) \right] \dot{\theta}_2^{\,2}$$

$$+ \left[1332 \left(\frac{\cos\beta}{1-\sin^2\beta\sin^2\theta_2} (\tan^{-1}(\tan\theta_2\cos\beta)) \right) \right]$$

$$- \left[1332 \left(\frac{\cos\beta}{1-\sin^2\beta\sin^2\theta_2} \right) \right] = 0.33 \ T_M \qquad (4.1)$$

and,

$$0.628 \ \ddot{\theta}_4 + 12000 \ \theta_4 - 12000 \ \tan^{-1}(\tan\theta_2\cos\beta) = 0. \qquad (4.2)$$

The value of the motor torque T_M depends upon the
specific motor constants and the field current I_f. The
equation relating T_M and I_f is derived in Appendix B and
is as follows:

$$T_M = 864 \; I_f^2 - 38.52 \; \dot{\theta}_2 \; I_f^2. \tag{4.3}$$

Equations (4.1) and (4.2) are simultaneous differential equations of second order and are highly nonlinear. A closed form solution was not found; hence, a numerical approach was followed. A fourth order Runge-Kutta method [5] was employed through the use of the IBM 360/50 computer. With the zero initial conditions, the equations of motion were solved for the following three cases:

Case 1.   The steady state constant level motor speed was chosen to be approximately 1200 rpm. This motor speed corresponds to a flywheel speed of 400 rpm which is equivalent to 6.67 rev/sec or 42 rad/sec. At this speed, the frequency of variation in the angular velocity at the specimen is about fourteen cps, assuming the input velocity ω_2 remains nearly constant.

The motor speed was varied by changing the field current from 0 to 0.5 ampere, in the equation of motion, in a manner as shown in Fig. 4.1. What this shows is that the field current was started at zero and increased linearly to a maximum value of 0.5 ampere in one second and then held constant. Equations (4.1) and (4.2) were solved for $\beta = 5^\circ$ and $\beta = 10^\circ$ to obtain a comparison of the effect of the angle β upon the total system response.
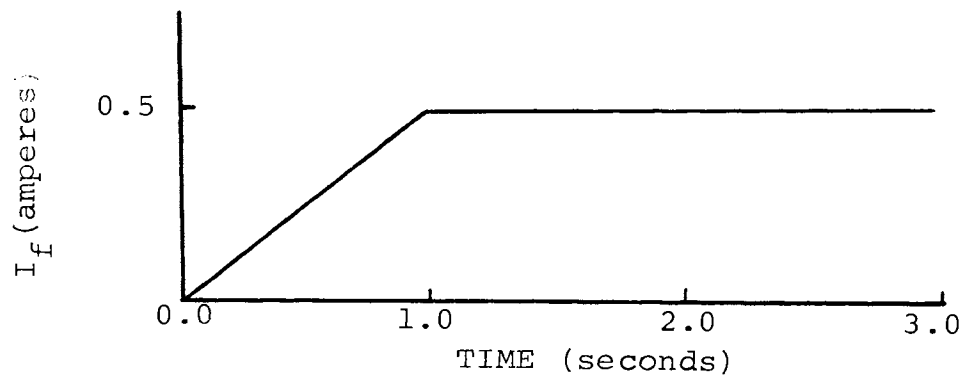
Fig. 4.1   Field Current - Time

Case 2.   The system constants are the same as Case 1 but the appropriate motor constants were chosen to result in a maximum motor speed of approximately 1800 rpm.   This corresponds to a flywheel speed of 600 rpm which is equivalent to 10 rev/sec or 62.8 rad/sec.   At this speed, the frequency of variation at the specimen should be about twenty cps.

The time varying input function for Eq. (4.1), the field current, was changed in the same manner as Case 1, but to a maximum value of 0.354 ampere. Angle β was taken as 5°.   These equations were solved to check the effect upon the system response when the frequency of variation in the angular velocity at the specimen was near the fundamental resonant frequency of the specimen.

Case 3.   This case is identical to Case 1 except that the flywheel inertia was increased by a factor of four and the equations were solved for $\beta = 5^\circ$.   This changes the value

of the coefficient of the $\ddot{\theta}_2$ term in Eq. (4.1). The
equations were solved in this case to compare the effect
of increased flywheel inertia.

B.   General Discussion of Results

In the absence of an analytical solution, the
numerical solutions have been compared with the physical
behavior that can be expected from the actuator. The
system response was evaluated for various values of para-
meters β, flywheel inertia I_F, and field current I_f.
These results are compared with each other to check the
behavior of the actuator for consistency.

Since a D.C. shunt motor is used as the prime mover,
the motor speed and, hence, the flywheel speed should
reach a steady state speed when started from rest. The
steady state speed will primarily depend upon the motor
constants and the field current I_f. For different values
of the field current I_f, different steady state flywheel
speeds may be expected.

A plot of $\dot{\theta}_2$ as a function of time for $\beta = 5^\circ$ and a
motor speed of approximately 1200 rpm is shown in Figure
4.2. This motor speed corresponds to the flywheel speed
of 400 rpm which is equivalent to 42 rad/sec. From the
graph it is observed that the flywheel starts from rest
and reaches, in about four seconds, the steady state speed
of 44.86 rad/sec which is 6.8% higher than expected.

$\beta = 5^\circ$, $I_F = 20.0$
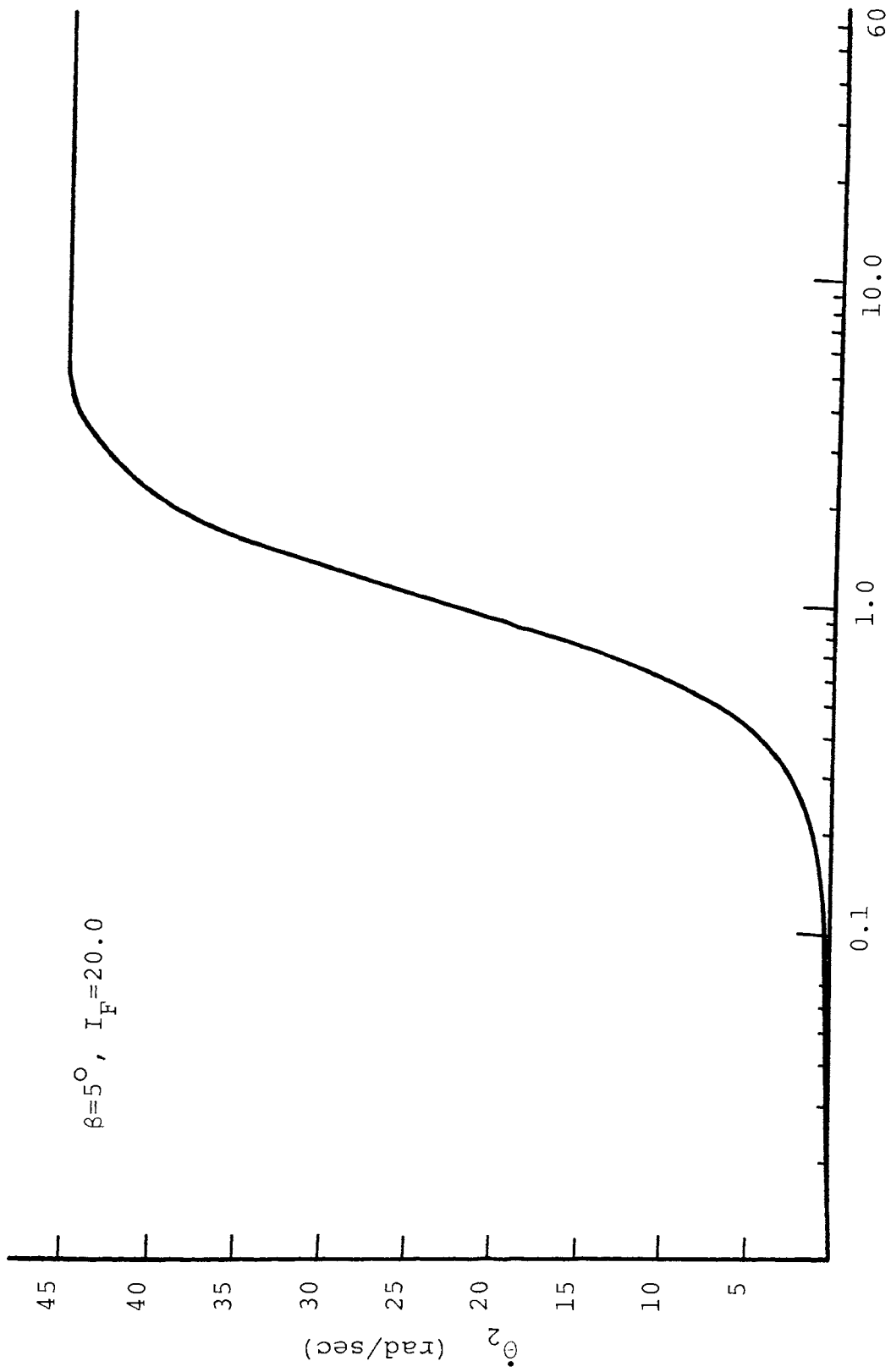
TIME (seconds)

Fig. 4.2 $\dot{\theta}_2$-TIME

$\dot{\theta}_2$ (rad/sec)

Because of the Hooke's joint, as seen in Fig. 2.2, the input speed variations to the specimen were expected to be approximately sinusoidal. Moreover, from the theory of undamped forced vibrations, it is anticipated that the variations in the angular speed of the specimen disc must also be approximately sinusoidal with a frequency equal to that of the input. A plot of $\dot{\theta}_4$ as a function of time in the steady state region for $\beta = 5^\circ$ and the motor speed of 1200 rpm is shown in Fig. 4.3. The motor speed of 1200 rpm corresponds to the flywheel speed of approximately 7 rev/sec. As the frequency of the output speed variations of the Hooke's joint is approximately a second harmonic of the input speed, the frequency of variations in $\dot{\theta}_3$ must be about 14 cps and, therefore, the same must be true for $\dot{\theta}_4$. From the graph it is seen that the frequency of variations of $\dot{\theta}_4$ is 14 cps and is approximately sinusoidal.

As discussed before, the flywheel speed should be approximately constant. However, because the driven shaft has a periodic acceleration, a torque from the driven side is exerted on the flywheel. This can be expected to cause a change in the flywheel speed perturbing it from a constant value. Figure 4.4 shows a plot of $\dot{\theta}_2$ in the steady state region for $\beta = 5^\circ$ and a motor speed of 1200 rpm. It can be seen from the graph that the frequency of
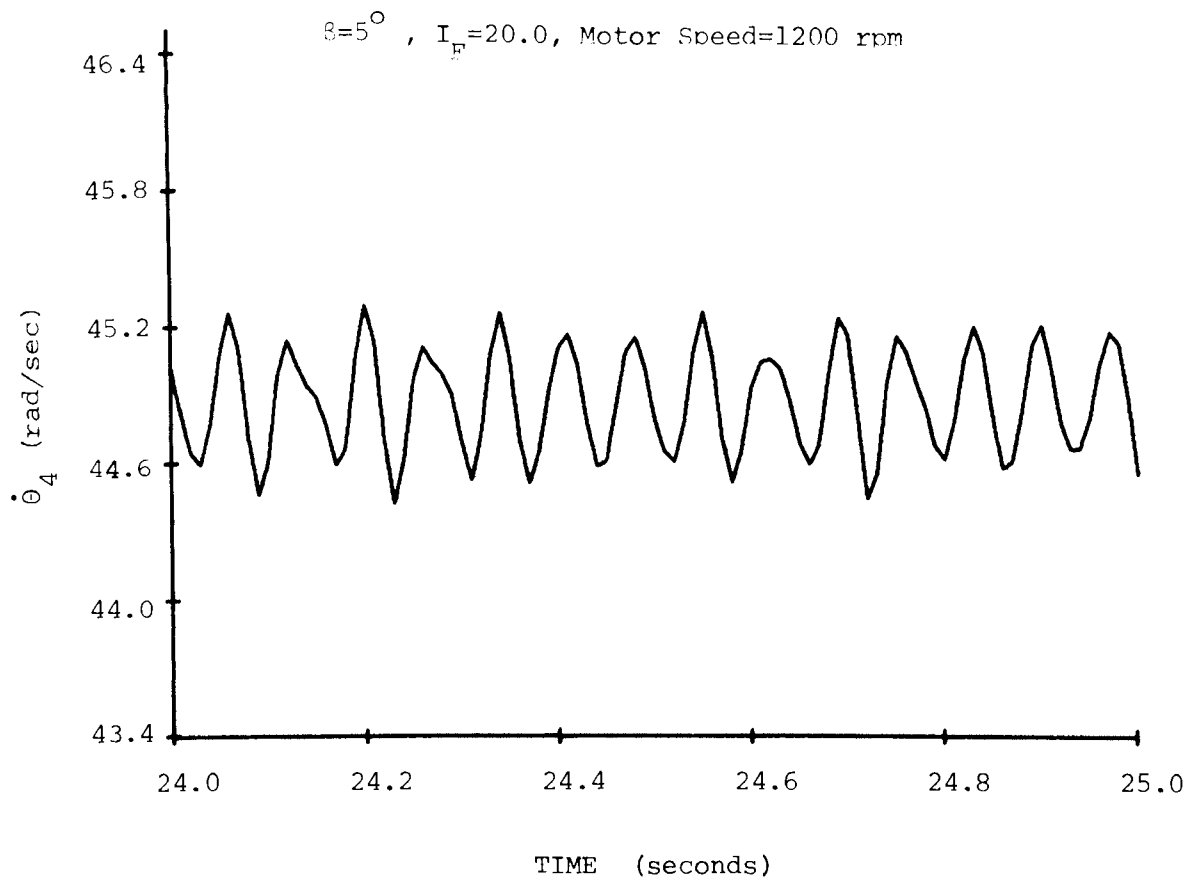
Fig. 4.3 $\dot{\theta}_4$-TIME
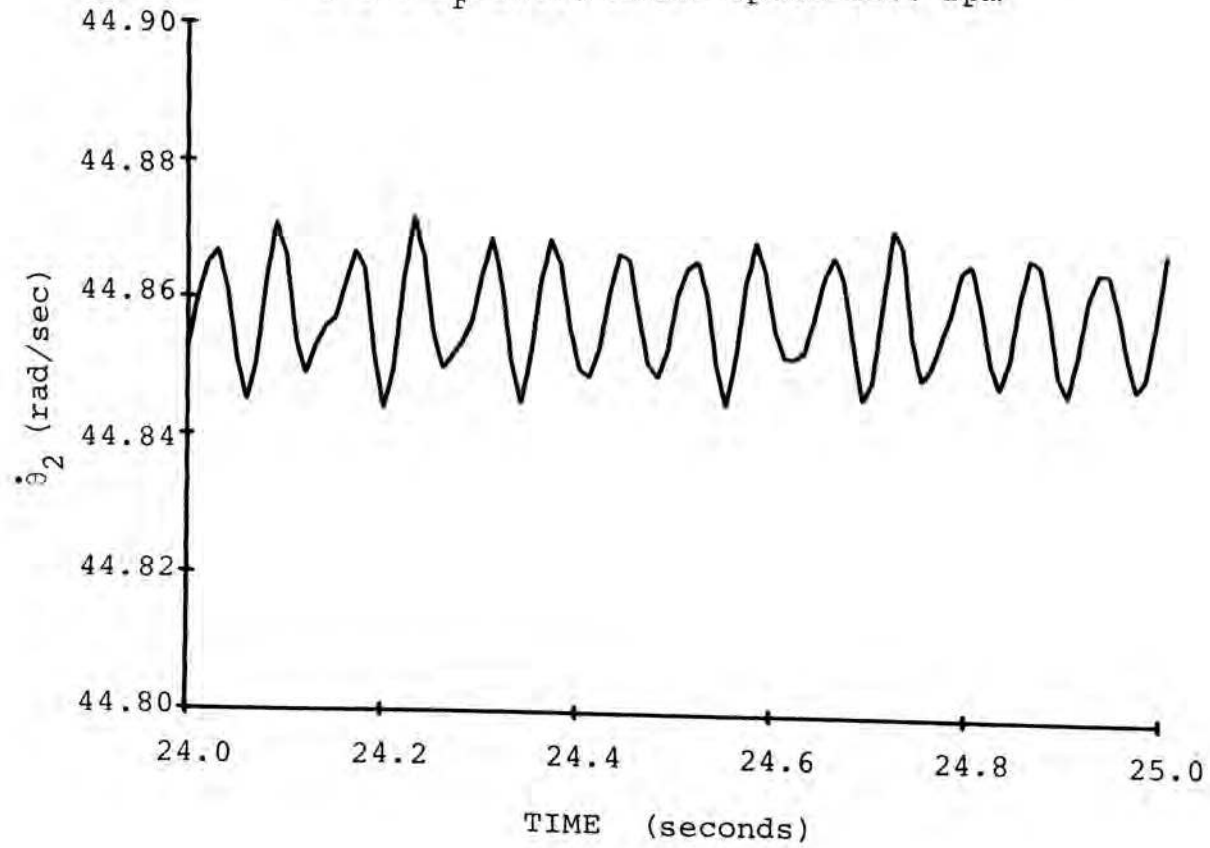
Fig. 4.4 $\dot{\theta}_2$-TIME

$\dot{\theta}_2$ is 14 cps and also the waveform of the variations is similar to that for $\dot{\theta}_4$ which is approximately sinusoidal. These results agree reasonably well with the expected physical behavior of the actuator. It may be noted that the average amplitude of $\dot{\theta}_2$ is very much smaller than that for $\dot{\theta}_4$ on account of the flywheel inertia.

C. Accuracy Comparison

In the Runge-Kutta method for the solution of the differential equations with the given initial conditions, the functional values are evaluated at the specified intervals called the step size. The accuracy [6], i.e., the maximum bound on the error with which the functional values are to be evaluated at each step, has also to be specified. In the calculation of these values, if the functional differences are greater than the specified accuracy criterion, the step size is halved and the new values of the functions are calculated until the accuracy requirement is met; this requires more time for computation. The above procedure is repeated at every step. The higher the accuracy requirement, the longer will be the time required for the calculation.

Initially, the actuator response from 0 to 10 seconds was found with an accuracy of 10^{-4}. The time required for the computation was about ten minutes. Although the steady state speed was reached in about four seconds, it was decided to obtain the system response from 0 to 25

seconds for all the cases. For this reason, it was
desirable that the time required for the computation be
reduced by some means. Therefore, the equations of motion
were also solved with the accuracy of 10^{-3} and 10^{-2}. The
time required for the computation with the accuracy of 10^{-3}
was about six minutes and that for the accuracy of 10^{-2}
was about three minutes for the system response upto
twenty five seconds. The results of $\dot{\theta}_2$ and $\dot{\theta}_4$ were com-
pared for the three different accuracy criteria which
are given in Table V and Table VI, respectively.

It can be noticed from the tables that even with
10^{-2} accuracy, the results are within 0.25 percent of those
with 10^{-4} accuracy. Hence, it was decided to solve the
equations of motion for all the different cases with 10^{-2}
accuracy. Considerable saving in the computer time was
thereby made without affecting the accuracy of the results
appreciably.

D.   Comparison of $\dot{\theta}_2$ for Various Values of β

In Fig. 4.1, it is observed that the flywheel takes
about four seconds to reach a level within 0.25 percent
of the mean steady state speed when $\beta = 5^\circ$. In order to
check the effect of the angle β on the rate of $\dot{\theta}_2$ reaching
a steady state speed, the equations of motion were solved
for $\beta = 0^\circ$ and $\beta = 10^\circ$, keeping all the other parameters
unchanged. Table VII shows the values of $\dot{\theta}_2$ for various

TABLE V

COMPARISON OF $\dot{\theta}_2$ FOR DIFFERENT ACCURACY REQUIREMENTS
$\beta=5^{\circ}$, $I_F=20.0$ lb. in. sec^2, and MOTOR SPEED=1200 rpm.

TIME	Accuracy Requirement*		
	10^{-4}	10^{-3}	10^{-2}
(seconds)	$\dot{\theta}_2$ (rad/sec)		
0.00	0.0	0.0	0.0
0.25	1.933	1.933	1.933
0.50	7.501	7.501	7.501
0.75	15.743	15.571	15.571
1.00	23.924	23.924	23.778
1.25	30.051	30.051	29.949
1.50	34.339	34.378	34.304
1.75	37.401	37.439	37.390
2.00	39.585	39.609	39.572
2.25	41.135	41.150	41.124
2.50	42.222	42.238	42.224
2.75	42.980	42.992	42.981
3.00	43.544	43.551	43.543
3.25	43.909	43.919	43.917
3.50	44.200	44.207	44.203
3.75	44.377	44.383	44.383
4.00	44.525	44.535	44.535
4.25	44.613	44.615	44.615
4.50	44.687	44.698	44.700
4.75	44.732	44.735	44.734
5.00	44.767	44.774	44.779

* Accuracy with which $\dot{\theta}_2$ is calculated

TABLE VI

COMPARISON OF $\dot{\theta}_4$ FOR DIFFERENT ACCURACY REQUIRMENTS
$\beta=5^{\circ}$, $I_F=20.0$ lb. in. $\sec^2$, and MOTOR SPEED=1200 rpm.

TIME	Accuracy Requirement*		
	10^{-4}	10^{-3}	10^{-2}
(seconds)	$\dot{\theta}_4$ (rad/sec)		
0.0	0.0	0.0	0.0
0.25	1.922	1.922	1.922
0.50	7.523	7.523	7.523
0.75	15.776	15.595	15.595
1.00	23.835	23.837	23.704
1.25	29.931	29.926	29.814
1.50	34.486	34.472	34.450
1.75	37.531	37.653	37.576
2.00	39.853	39.775	39.797
2.25	41.035	41.079	41.137
2.50	42.011	42.057	41.980
2.75	43.284	43.260	43.237
3.00	43.215	43.294	43.323
3.25	44.256	44.183	44.116
3.50	43.898	43.949	43.995
3.75	44.614	44.652	44.607
4.00	44.361	44.265	44.272
4.25	44.733	44.875	44.900
4.50	44.634	44.485	44.428
4.75	44.817	44.873	44.961
5.00	44.744	44.746	44.629

* Accuracy with which $\dot{\theta}_4$ is calculated

TABLE VII

COMPARISON OF $\dot{\theta}_2$ FOR VARIOUS β ANGLES

I_F=20.0 lb. in. sec^2 and MOTOR SPEED=1200 rpm.

TIME	Angle β (degrees)		
	0	5	10
(seconds)	$\dot{\theta}_2$ (rad/sec)		
0.0	0.000	0.000	0.000
0.25	1.933	1.933	1.934
0.50	7.501	7.501	7.500
0.75	15.571	15.571	15.569
1.00	23.776	23.778	23.786
1.25	29.945	29.949	29.962
1.50	34.309	34.304	34.291
1.75	37.396	37.390	37.375
2.00	39.579	39.572	39.511
2.25	41.124	41.124	41.157
2.50	42.217	42.224	42.257
2.75	42.989	42.981	42.965
3.00	43.536	43.543	43.580
3.25	43.923	43.917	43.893
3.50	44.196	44.203	44.233
3.75	44.390	44.383	44.359
4.00	44.527	44.535	44.560
4.25	44.624	44.615	44.594
4.50	44.692	44.700	44.715
4.75	44.741	44.734	44.726
5.00	44.775	44.779	44.775
10.00	44.858	44.853	44.827
15.00	44.858	44.865	44.890
20.00	44.858	44.849	44.841
25.00	44.858	44.868	44.821

values of β at the different instant of time upto twenty

five seconds.

It can be observed from this table that even for

different values of β, the value of $\dot{\theta}_2$ at the same instant

of time, is the same within a fraction of one percent.

Hence, it can be concluded that the time required for the

system to reach the steady state level is independent of

angle β, for reasonably moderate values of β.

E.   Comparison of System Response for Two Values of β

In order to check the effect of angle β on the system

response, the equations of motion were solved for β = 5°

and β = 10°. The plots of $\dot{\theta}_2$ and $\dot{\theta}_4$ against time in the

steady state region for β = 10° are shown in Fig. 4.5 and

Fig. 4.6, respectively. Comparing these figures with

Fig. 4.3 and Fig. 4.4, it can be observed that the ampli-

tudes of variation increase with the angle β, both for

$\dot{\theta}_2$ and $\dot{\theta}_4$ as expected from the kinematics of the Hooke's

joint. It may also be noticed that the variations in

$\dot{\theta}_2$ and $\dot{\theta}_4$ are approximately sinusoidal and have the same

frequency.

The values of the average peak amplitudes of $\dot{\theta}_2$, $\dot{\theta}_3$

and $\dot{\theta}_4$ for various values of β are tabulated in Table VIII.

The amplitudes of the variation of $\dot{\theta}_2$ and $\dot{\theta}_4$ are found from

the numerical results of the system response. The ampli-

tude of variation of $\dot{\theta}_3$ is calculated from the kinematic

relationship of the Hooke's joint. Assuming $\dot{\theta}_2$ to be a

$\beta=10^{O}$, $I_F=20.0$, Motor Speed=1200 rpm
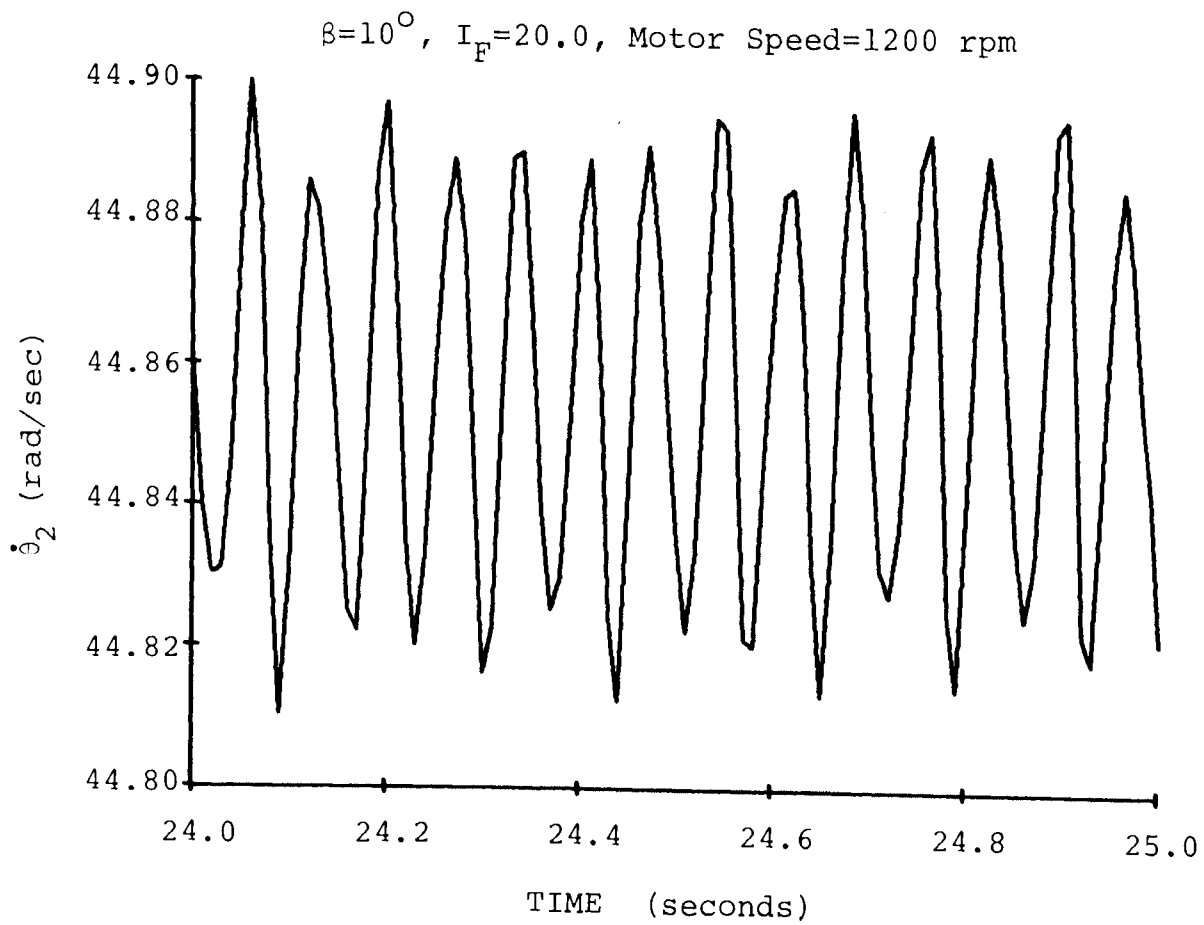
Fig. 4.5 $\dot{\vartheta}_2$-TIME

$\beta=10^{\circ}$, $I_F=20.0$, Motor Speed=1200 rpm
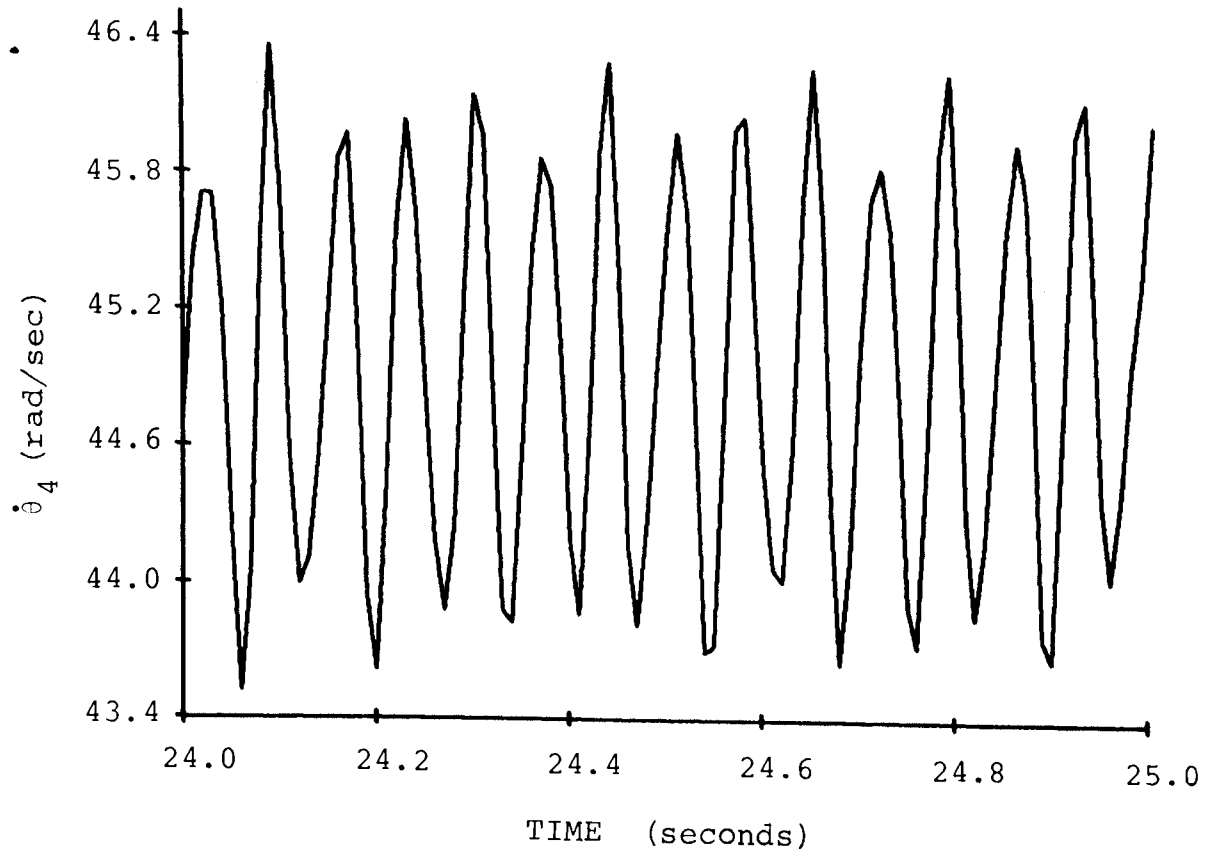
Fig. 4.6 $\dot{\theta}_4$- TIME

TABLE VIII

COMPARISON OF $\dot{\theta}_2$, $\dot{\theta}_3$ AND $\dot{\theta}_4$ FOR

TWO VALUES OF β

I_F=20.0 lb. in. sec^2 and MOTOR SPEED=1200 rpm

Time Interval (seconds)	$\beta=5^{\circ}$		$\beta=10^{\circ}$	
	Frequency (cps)	Amplitude*	Frequency (cps)	Amplitude*
$\dot{\theta}_2$ (rad/sec)				
14-15	14	0.102	14	0.036
24-25	14	0.010	14	0.037
$\dot{\theta}_3$ (rad/sec)				
14-15	14	0.170	14	0.690
24-25	14	0.171	14	0.690
$\dot{\theta}_4$ (rad/sec)				
14-15	14	0.314	14	1.180
24-25	14	0.322	14	1.256

* Average of Peak Values

constant, the peak amplitudes of $\dot{\theta}_3$ have been shown in
Table I for various values of β. For example, the
average value of $\dot{\theta}_2$ for $\beta = 5°$ and the motor speed of 1200
rpm as found from the numerical results is 44.86 rad/sec
(see Fig. 4.4). From Table I,

$$\text{Peak amplitude of } \dot{\theta}_3 = 0.00381 \ \dot{\theta}_2$$

$$= 0.00381 \times 44.86 = 0.17.$$

Since the variations in $\dot{\theta}_3$ are not exactly sinusoidal,
the average of the peak values have been used.

The equations of motion were also solved for $\beta = 0°$.
From the numerical results, it was observed that $\dot{\theta}_4$ was
almost constant with minor perturbations at somewhat
regular intervals. These perturbations were within five
percent of the average amplitude of $\dot{\theta}_4$ for $\beta = 5°$ for the
same motor speed of 1200 rpm. However, from the kinematic
relationship of the Hooke's joint $\dot{\theta}_3$ and, hence, $\dot{\theta}_4$ must
be constant. These perturbations appear to be caused by
propagated errors in the numerical solution.

It was also observed that $\dot{\theta}_2$ was almost constant due
to the absence of pulsating inertia load torque. Moreover,
the steady state flywheel speed $\dot{\theta}_2$ was the same as that
attained when the angle β was $5°$. The graph of $\dot{\theta}_2$ for
$\beta = 0°$ was very much similar to the one for $\beta = 5°$ which
is shown in Fig. 4.2 This agrees with the expected physical
behavior of the actuator.

F.   Comparison of System Response for Two Values of
     Motor Speed

In addition to the previous comparisons, the effect
of changes in the motor speed on the frequency and the
amplitude of variation of $\dot{\theta}_2$ and $\dot{\theta}_4$ was examined. The
speed of the motor could be varied by means of the field
current control. The system response was found for a
motor speed of approximately 1800 rpm which corresponds to
the flywheel speed of 10 rev/sec which is equivalent to
62.8 rad/sec. Hence, the frequency of variation of $\dot{\theta}_3$
and $\dot{\theta}_4$ must be 20 cps as it is the second harmonic of the
driver shaft speed.

Figures 4.7 and 4.8 show the graphs of $\dot{\theta}_2$ and $\dot{\theta}_4$ as
a function of time, respectively, in the steady state
region, for $\beta = 5^\circ$. It can be noticed from Fig. 4.7 that
the mean steady state flywheel speed is 63.35 rad/sec which
is 0.87 percent higher than the expected value of 62.8 rad/sec.
Also, it can be observed that the frequency of variation of
$\dot{\theta}_2$ and $\dot{\theta}_4$ is 20 cps and the variations are approximately
sinusoidal.

Comparing these figures with Fig. 4.3 and Fig. 4.4,
it can be observed that the amplitudes of variation in-
crease with an increase in the motor speed. This agrees
quite well with the kinematic relationship of the Hooke's
joint as seen from Eq. (2.3). The values of frequency and
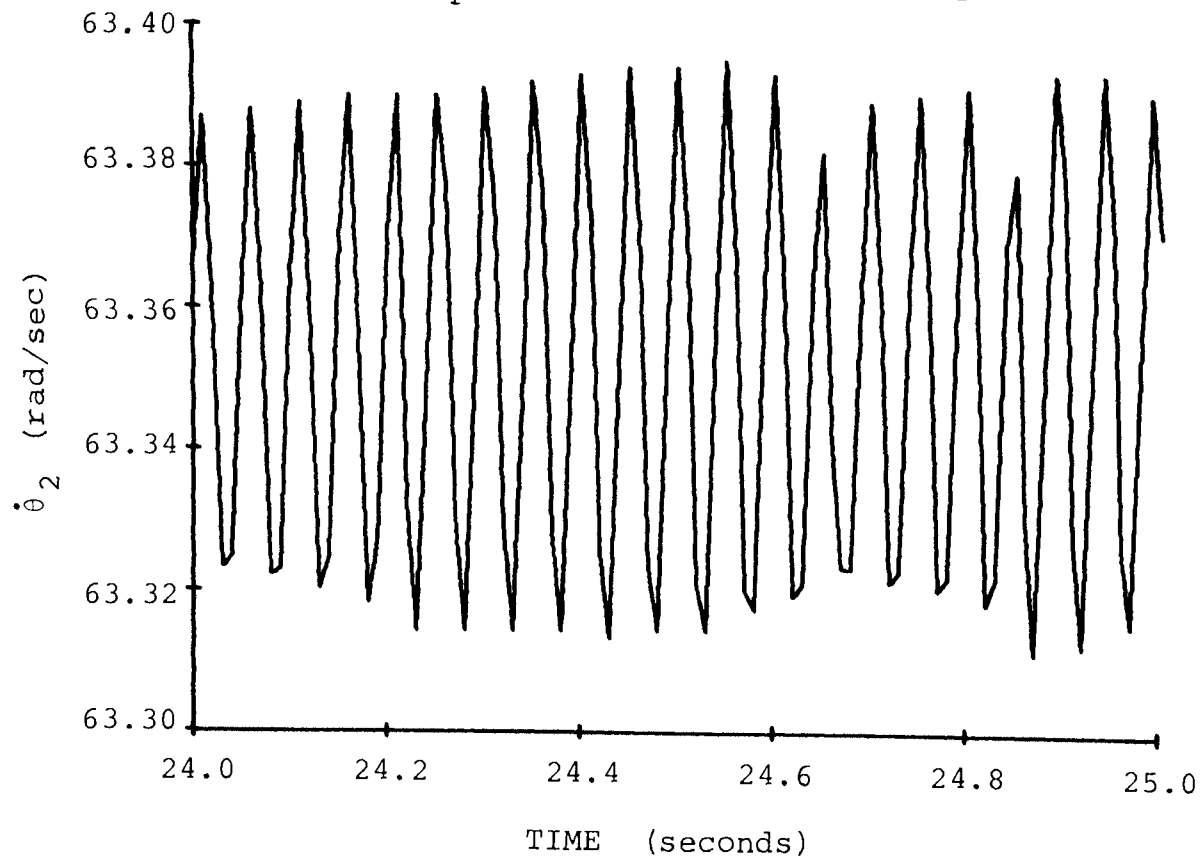
$\beta=5^{O}$, $I_F=20.0$, Motor Speed=1800 rpm
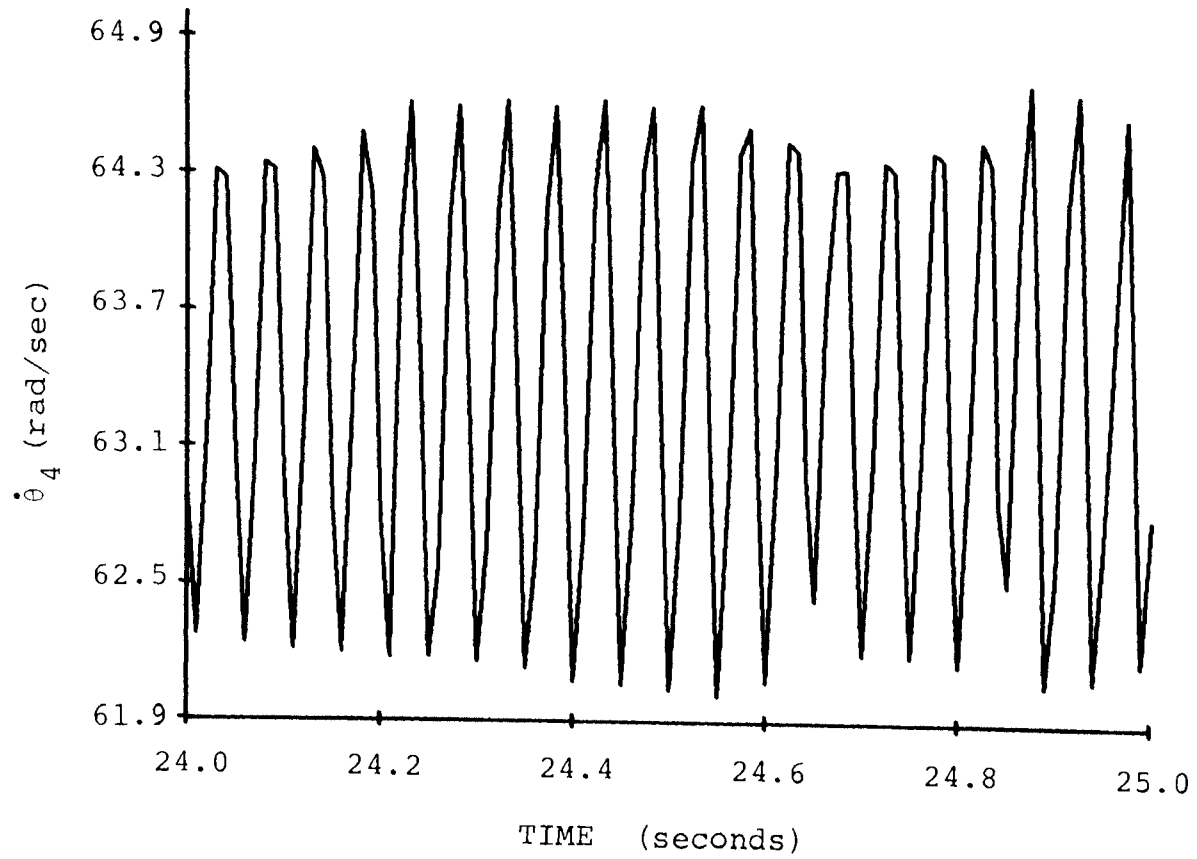
Fig. 4.7 $\dot{\theta}_2$- TIME

Fig. 4.8 $\dot{\theta}_4$ - TIME

the amplitude of variations in $\dot{\theta}_2$, $\dot{\theta}_3$ and $\dot{\theta}_4$ have been shown in Table IX for two values of the motor speed.

G.   Comparison of System Response for Two Values of Flywheel Inertia

To check the effect of an increase in the flywheel inertia on the system response, the equations of motion were solved for $\beta = 5^{\circ}$ and the motor speed of 1200 rpm when the flywheel inertia is increased by a factor of four. From the numerical results, it is observed that it takes about fifteen seconds for the flywheel to reach the steady state speed as compared to four seconds when the flywheel with the lower inertia ·was used. This appears reasonable as it takes a longer time to accelerate a larger inertia.

The plots of $\dot{\theta}_2$ and $\dot{\theta}_4$ in the steady state region are shown in Fig. 4.9 and Fig. 4.10, respectively. It can be observed from the plots that the frequency of variation is 14 cps and this time the waveform is very close to being sinusoidal. Comparing these figures with Fig. 4.3 and Fig. 4.4, it is noticed that the amplitude of variations of $\dot{\theta}_2$ decreases considerably and the peak amplitudes are only about 1/4 of those in the case when a flywheel with lower inertia was used. This means that the flywheel with larger inertia will minimize the amplitude of variations in $\dot{\theta}_2$. Because of this, it is observed that the variations in $\dot{\theta}_4$ are very symmetric and very close to being sinusoidal.

TABLE IX

COMPARISON OF $\dot{\theta}_2$, $\dot{\theta}_3$, $\dot{\theta}_4$ FOR

TWO VALUES OF MOTOR SPEED

$\beta=5^{\circ}$ and $I_F=20.0$ lb. in. sec^2

Time Interval (Seconds)	Motor Speed			
	1200 rpm		1800 rpm	
	Frequency (cps)	Amplitude*	Frequency (cps)	Amplitude*
$\dot{\theta}_2$ (rad/sec)				
14-15	14	0.102	20	0.039
24-25	14	0.010	20	0.037
$\dot{\theta}_3$ (rad/sec)				
14-15	14	0.170	20	0.241
24-25	14	0.171	20	0.241
$\dot{\theta}_4$ (rad/sec)				
14-15	14	0.314	20	1.254
24-25	14	0.322	20	1.180

* Average of Peak Values

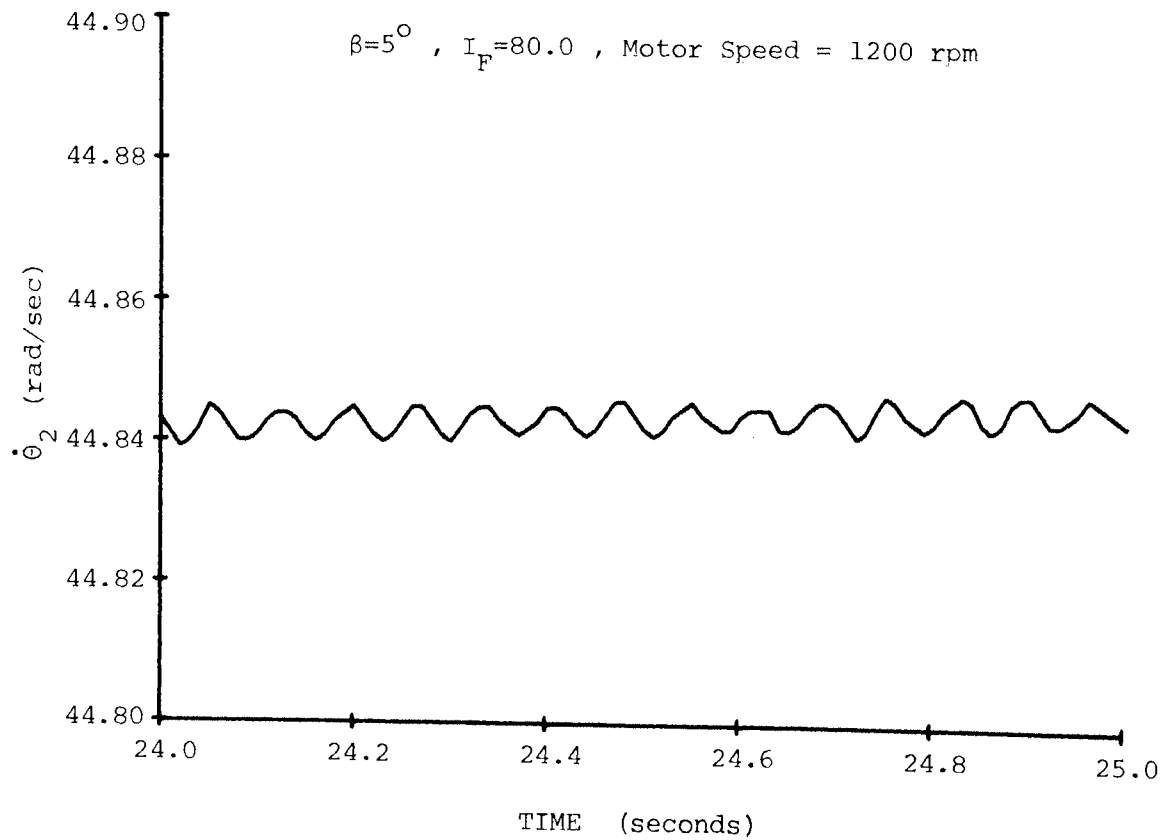$\beta = 5^{\circ}$, $I_F = 80.0$, Motor Speed = 1200 rpm

Fig. 4.9 $\dot{\theta}_2$ - TIME
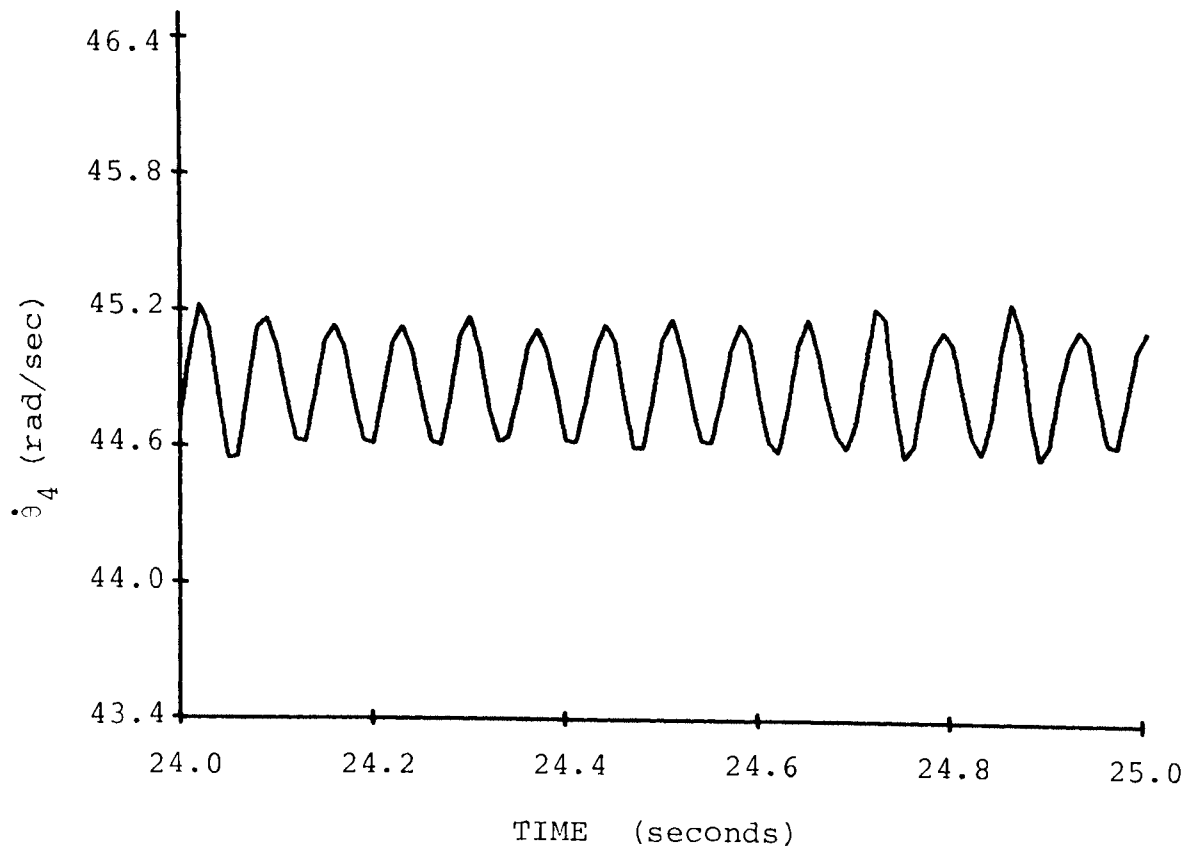
$\beta=5^{O}$, $I_F=80.0$, Motor Speed=1200 rpm

Fig. 4.10 $\dot{\theta}_4$- TIME

Also the amplitude of variations $\dot{\theta}_4$ decreases by about ten percent as the peaks are considerably more uniform.

H.   Summary of Results

The amplitudes of variation of $\dot{\theta}_2$, $\dot{\theta}_3$ and $\dot{\theta}_4$ in the steady state region for the different cases have been tabulated in Table X and the amplitude ratios of $\dot{\theta}_4/\dot{\theta}_3$ and $\dot{\theta}_4/\dot{\theta}_2$ have been listed. At the steady state, the amplitude ratio of $\dot{\theta}_4/\dot{\theta}_3$ can also be theoretically calculated for the undamped forced vibration of a one degree of freedom system [7], assuming that the input source of excitation is not affected by the reaction of the system. This result is:

$$\text{Amplitude ratio} \quad \frac{\dot{\theta}_4}{\dot{\theta}_3} = \frac{1}{1-(\frac{\omega}{\omega_n})^2}$$

where:

ω = Circular frequency of exciting force in rad/sec.

ω_n = Natural frequency of undamped vibration in rad/sec.

Substituting for $\omega = 2\Pi f$ and $\omega_n = 2\Pi f_n$ in the above equation gives:

$$\text{Amplitude ratio} \quad \frac{\dot{\theta}_4}{\dot{\theta}_3} = \frac{1}{1-(\frac{f}{f_n})^2} \qquad (4.4)$$

where:

f = Frequency of exciting force in cps

f_n = Natural frequency of undamped vibration in cps.

The natural frequency of the undamped torsional vibrations of the specimen used for the numerical analysis was 23 cps. The theoretical amplitude ratio of $\dot{\theta}_4/\dot{\theta}_3$ has been shown in the last column of Table X. Comparing this amplitude ratio with the one obtained from the numerical results (column 6, Table X), it is observed that the amplitude ratio $\dot{\theta}_4/\dot{\theta}_3$ obtained from the numerical results is higher than the theoretical value and is within twenty percent of it. This may be due to the fact that the driver speed was not exactly constant and, therefore, the variation in $\dot{\theta}_4$ are not expected to be sinusoidal. Hence, some uneven peaks appear which increase the amplitude of $\dot{\theta}_4$, thus, increasing the value of amplitude ratio $\dot{\theta}_4/\dot{\theta}_3$.

The case in which the flywheel inertia was 80 lb.in. $\sec^2$, the amplitude ratio $\dot{\theta}_4/\dot{\theta}_3$ as obtained from the numerical results was within five percent of the theoretical value. The reason for this is that the flywheel with a larger inertia reduces the variations in $\dot{\theta}_2$ to a minimum value; thus, the waveform of $\dot{\theta}_4$ is nearly sinusoidal. This confirms that the numerical results agree reasonably with the expected physical behavior.

It may be noticed that the amplitude ratio of $\dot{\theta}_4/\dot{\theta}_3$ for the frequency of input variations of 20 cps is about

TABLE X

COMPARISON OF THE AMPLITUDES OF $\dot\theta_2$, $\dot\theta_3$ AND $\dot\theta_4$ FOR THE DIFFERENT CASES

	Time Interval (seconds)	Amplitude* $\dot\theta_2$	Amplitude* $\dot\theta_3$	Amplitude* $\dot\theta_4$	Amplitude Ratio $\dot\theta_4/\dot\theta_3$	Amplitude Ratio $\dot\theta_4/\dot\theta_2$	Theoritical Amplitude Ratio $\dot\theta_4/\dot\theta_3$
Motor Speed (rpm)	$\beta=5^\circ$ and $I_F=20.0$ lb. in. sec^2						
1200	24-25	0.010	0.171	0.322	1.88	31.3	1.60
1800	24-25	0.037	0.241	1.180	4.90	32.1	4.17
β (degrees)	Motor Speed=1200 rpm and $I_F=20.0$ lb. in. sec^2						
5	24-25	0.010	0.171	0.322	1.88	31.3	1.60
10	24-25	0.037	0.690	1.256	1.82	34.4	1.60
I_F lb.in.sec^2	$\beta=5^\circ$ and Motor Speed=1200 rpm						
20.0	24-25	0.010	0.171	0.322	1.88	31.3	1.60
80.0	24-25	0.0024	0.171	0.2845	1.67	119.0	1.60

* Average of Peak Values

2 1/2 times greater than that for 14 cps. This is due to the fact that the amplitude ratio increases as the exciting frequency approaches the natural frequency of vibration, which is 23 cps in the present case.

It may also be noted from the table that the amplitude ratio $\dot\theta_4/\dot\theta_2$, except in the case when a larger flywheel inertia is used, is nearly equal for the cases considered. The reason seems to be that when the amplitude of variation of $\dot\theta_4$ increases either with an increase in the motor speed or an increase in the angle β, the inertia load torque also increases. This increases its effect on the flywheel speed and the amplitude of variation of $\dot\theta_2$ also increases. Hence, an increase in the amplitude of $\dot\theta_4$ is accompanied by the proportional increase in the amplitude of variation of $\dot\theta_2$, keeping the amplitude ratio $\dot\theta_4/\dot\theta_2$ nearly constant.

When a flywheel with the larger inertia is used, the flywheel speed is very nearly constant and hence, the amplitude of variations in $\dot\theta_2$ is so small that the amplitude ratio $\dot\theta_4/\dot\theta_2$ increases appreciably in this case by a factor of about four. This characteristic also confirms that the numerical results obtained agree well with the physical behavior that can be expected of the actuator.

In order to obtain the system response when the frequency of variation was above the natural frequency of the specimen, the equations of motion were solved for $\beta = 5^\circ$

and $I_f = 0.252$ ampere. For this case the frequency of excitation was about 33 cps. It was observed that both $\dot{\theta}_2$ and $\dot{\theta}_4$ increased from 0 to about 68 rad/sec in a manner similar to the case in which the frequency of variation was about 20 cps. However, from that point on, for a certain period of time, the amplitudes of both $\dot{\theta}_2$ and $\dot{\theta}_4$ became very large. The reason for this behavior is that $\dot{\theta}_2 = 68$ rad/sec corresponds to the frequency of 21.5 cps. This frequency is very near to the calculated natural frequency of the specimen which is 23 cps.

From the numerical results it was found that the amplitude ratio $\dot{\theta}_4/\dot{\theta}_3$ in the resonance region was 36.0. The amplitude ratio $\dot{\theta}_4/\dot{\theta}_3$ in the steady state region was 4.90 when the frequency of excitation was about 20 cps, all other parameters being the same. Comparing these two values, it is observed that the numerical results agree closely with the results expected from the theory of forced vibration (see Eq. 4.4).

After passing through the resonance region in the numerical solutions, the amplitudes of variation of $\dot{\theta}_2$ and $\dot{\theta}_4$ decrease. In the steady state region, when the frequency of excitation was about 33 cps, the amplitude ratio $\dot{\theta}_4/\dot{\theta}_3$ was found to be 0.59. This qualitatively agrees with the results expected from the theory of forced vibration, i.e., the amplitude ratio is less than unity when the forcing frequency is well above the natural frequency of the system.

In an early set of numerical solutions, the equations of motion were solved for all the three cases using a lower value of the motor torque T_M than the one given by Eq. (B.9). A comparison of these results was made with the present set of results in which the value of T_M used was as given by Eq. (B.9). It was found from this comparison that in the previous set, the system took a longer time to reach the steady state speed, since the motor exerted a low torque. However, the steady state speed reached in the different cases were nearly the same as in the corresponding cases in the present set. This was expected as the same motor characteristics except the different values of T_M were used. This also suggests that the numerical method yielded reasonably consistent results.

CHAPTER V

CONCLUSIONS AND RECOMMENDATIONS

From the numerical solutions to the equations of
motion, for the variations of parameters considered, the
following conclusions can be drawn:

1. The time required to reach steady state speed
    is nearly independent of the angle β when
    the other system parameters are held constant.
    However, this time interval increases when the
    flywheel inertia is increased, i.e., the larger
    the flywheel inertia, the longer will be the
    time required to attain steady state speed.

2. Increasing angle β for a given constant motor
    speed , causes the average amplitude of the speci-
    men angular velocity to increase. The frequency
    of variation in the specimen angular velocity
    is approximately a second harmonic of the fly-
    wheel speed when steady state conditions are
    reached. This frequency is nearly independent
    of angle β if the other system parameters remain
    constant.

3. The average amplitude of variations in the fly-
    wheel angular velocity decreases with an increase
    in the flywheel inertia, other parameters remaining
    fixed. In addition, the specimen angular velocity
    is more regular and more nearly sinusoidal when
    the flywheel inertia is increased.

4. The system examined is feasible as a torsional
    vibration exciter. The amplitude of output vibra-
    tions can be controlled by variation in the Hooke's
    joint angle or the motor speed. The frequency of
    vibration is controlled only by the motor speed.

5. The numerical results presented herein were all
    obtained with a step size of 0.01 sec. This tends
    to cause the waveforms of both $\dot{\theta}_2$ and $\dot{\theta}_4$ to be
    somewhat irregular because only a few points per
    cycle are available. Hence, the equations of motion
    should be solved using a smaller step size and the
    results compared to observe the effect of the step
    size on the regularity of the waveforms of $\dot{\theta}_2$ and
    $\dot{\theta}_4$.

6. The equations of motion were solved for only three
    different motor speeds. To obtain the system
    response over a wider range of vibration frequen-
    cies, the equations should be solved for a greater
    range of motor speeds.

CHAPTER VI

APPENDICES

Appendix A

FUNDAMENTAL FREQUENCY ROOT CALCULATION
FOR THE TORSIONAL SPECIMEN

A procedure used to find the first natural frequency
root of a system as shown in Figure A.1 is given by
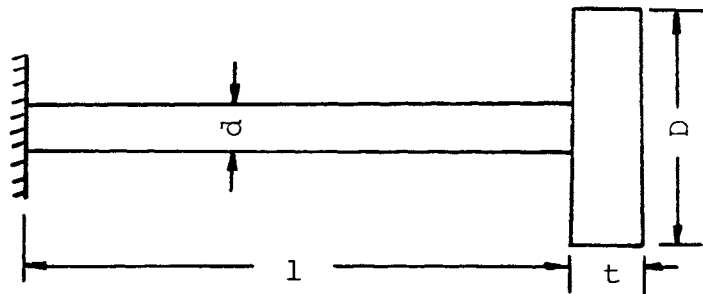Volterra [4], and the same has been used here.

Fig. A.1 Specimen

The frequency equation for this system is:

$$\gamma \tan \gamma = \alpha \qquad (A.1)$$

In this transcendental equation,

$$\gamma = \frac{\omega l}{a}$$

where:

ω = Frequency of vibration (rad/sec)

l = Length of elastic shaft

$$a^2 = GJ/I_p$$

GJ = Torsional rigidity of shaft

I_p = Mass moment of inertia of shaft.

The value of α for torsional vibrations [8] is given as:

$$\alpha = \frac{\text{Mass moment of inertia of shaft}}{\text{Mass moment of inertia of disc}} \ .$$

Assuming both the shaft and the disc to be made of the same material,

$$\alpha = \frac{d^4 l}{D^4 t} \ .$$

Substituting the value of α into Eq. (A.1) gives:

$$\gamma \tan \gamma = \frac{d^4 l}{D^4 t} \ . \tag{A.2}$$

An approximate value of the lowest root γ_1 is obtained as follows. When the mass moment of inertia of the shaft is very small as compared to that of the disc, the ratio α and root γ_1 are also very small quantities and $\tan \gamma_1$ is approximately equal to γ_1. Therefore, Eq. (A.2) can be written as:

$$\gamma_1{}^2 \approx \frac{d^4 l}{D^4 t} \ . \tag{A.3}$$

From the dimensions of the specimen, the value of γ_1 can be found. From this the approximate lowest natural

frequency can be found from:

$$f_1 = \frac{\gamma_1}{2\pi l}\sqrt{\frac{Gg}{\rho}} \qquad \text{(A.4)}$$

where:

f_1 = Approximate lowest natural frequency

G = Modulus of rigidity of the shaft

g = Gravitational constant

l = Length of the shaft

ρ = Weight density per unit volume of the shaft.

From Eq. (A.3) and Eq. (A.4), it may be noted that natural frequency is directly proportional to shaft diameter d, and inversely proportional to shaft length l, disc thickness t, and disc diameter D.

APPENDIX B

MOTOR TORQUE EQUATION

For a D.C. shunt motor [9],

$$I_a = \frac{V-E}{R_a} \tag{B.1}$$

where:

I_a = Armature current

V = Line voltage

E = Back e.m.f.

R_a = Armature resistance.

Also, the back e.m.f. developed by the armature is given by:

$$E = K_1 \tilde{\phi} S \tag{B.2}$$

where:

K_1 = A constant

$\tilde{\phi}$ = Total flux entering the armature from one north pole

$S = \dot{\theta}_1$ = Speed of armature.

The flux $\tilde{\phi}$ is proportional to the field current I_f.

$$\therefore \tilde{\phi} = K_2 I_f \tag{B.3}$$

where K_2 is a constant. Substituting for $\tilde{\phi}$ from Eq. (B.3) and using $S = \dot{\theta}_1$ in Eq. (B.2) gives:

$$E = K_1 K_2 I_f \dot{\theta}_1 = \widehat{K} \, I_f \, \dot{\theta}_1 \qquad\qquad (B.4)$$

where $\widetilde{K} = K_1 K_2$ is a constant.

The equation for torque T_M developed by the motor is:

$$T_M = K_3 \, I_a \, \widetilde{\phi} \qquad\qquad (B.5)$$

Substituting for $\widetilde{\phi}$ from Eq. (B.3) into Eq. (B.5) gives:

$$T_M = K_3 K_2 I_a I_f, \text{ or}$$

$$T_M = K_t \, I_a \, I_f \qquad\qquad (B.6)$$

where $K_t = K_2 K_3$ is constant. Substituting for E from Eq. (B.4) into Eq. (B.1) gives:

$$I_a = \frac{V - \widetilde{K} I_f \dot{\theta}_1}{R_a} \quad . \qquad\qquad (B.7)$$

Substituting for I_a from Eq. (B.7) into Eq. (B.6) gives an expression for motor torque T_M as:

$$T_M = K_t \, I_f \left(\frac{V - \widetilde{K} \, I_f \, \dot{\theta}_1}{R_a} \right) .$$

$$\therefore \; T_M = \frac{K_t \, I_f \, V}{R_a} - \frac{K_t \, \widetilde{K} \, I_f^{\,2}}{R_a}. \qquad\qquad (B.8)$$

This is the required equation for the torque T_M developed by the D.C. shunt motor.

The values of the constants $\widetilde{K}$, K_t and R_a for a 1/2
h.p., 125 volts D.C. shunt motor must be established. In
evaluation of these constants, some of the values, such
as overall efficiency, voltage drop etc., have been assumed,
which are quite appropriate to the general specifications
of these type of motors. Assuming an overall efficiency
of the motors as 80% and noting that 1 h.p. = 746 watts,
at full load,

$$\text{Power input} = \frac{1/2 \times 746}{0.8}$$

$$= 466 \text{ watts}$$

and,

$$\text{Armature current } I_a = \frac{\text{Power Input}}{\text{Line Voltage}}$$

$$= \frac{466}{125} = 3.75 \text{ amperes.}$$

Assuming the voltage drop across the armature at full
load equal to 6% of line voltage,

Voltage drop across the armature
at full load = 0.06 x 125 = 7.5 volts.

$$\text{Armature resistance, } R_a = \frac{\text{Voltage drop at full load}}{\text{Armature current at full load}}.$$

$$\therefore R_a = \frac{7.5}{3.75} = 2 \text{ ohms.}$$

Also, back e.m.f. = Line voltage - Voltage drop.

$$\therefore E = 125 - 7.5 = 117.5 \quad \text{volts.}$$

The equation relating h.p., torque in lb.ft. and speed in rpm is:

$$\text{h.p.} = \frac{2\Pi \ NT}{33,000} \ .$$

$$\therefore \ T = \frac{\text{h.p. } \times \ 33,000}{2\Pi \ N} \ .$$

For 1/2 h.p. motor running at 1200 rpm,

$$T = \frac{1/2 \times 33,000}{2\Pi \times 1200} = 2.20 \ \text{lb.ft.}$$

$$\therefore T = 26.4 \ \text{lb.in.}$$

But from Eq. (B.6),

$$T = K_t \ I_a \ I_f.$$

Assuming the field current $I_f = 0.5$ ampere for the motor speed of 1200 rpm, and equating two torque equations, gives:

$$26.4 = K_t \times 3.75 \times 0.5$$

$$\therefore K_t = 13.8.$$

Also, from Eq. (B.4),

$$E = \tilde{k} \ I_f \ \dot{\theta}_1 \ .$$

$$\therefore \widetilde{k} = \frac{E}{I_f \, \dot{\theta}_1} \, .$$

$$\therefore \widetilde{k} = \frac{117.5}{0.5 \times [\frac{1200 \times 2\Pi}{60}]} = 1.87.$$

From Eq. (3.7),

$$\dot{\theta}_1 = \frac{\dot{\theta}_2}{n}$$

Where, n = Pulley ratio = 0.33.

$$\therefore \dot{\theta}_1 = \dot{\theta}_2/0.33.$$

From Eq. (B.8), the torque T_M developed by the motor is given as:

$$T_M = \frac{K_t \, I_f \, V}{R_a} - \frac{K_t \, \widetilde{k} \, I_f^2 \, \dot{\theta}_1}{R_a}$$

Substituting the values of $\widetilde{k}$, K_t, R_a and $\dot{\theta}_1$ in the above equation,

$$T_M = \frac{13.8 \times I_f \times 125}{2} - \frac{13.8 \times 1.87 \times I_f^2 \times \dot{\theta}_2/0.33}{2}$$

$$\therefore T_M = 864 \, I_f - 38.52 \, \dot{\theta}_2 \, I_f^2. \tag{B.9}$$

Equation (B.9) represents the governing motor torque, speed equation.

CHAPTER VII

BIBLIOGRAPHY

1. Halsey, F.A., "Handbook for Machine Designers",
    McGraw-Hill Book Company, Inc., New York, second
    edition, 1969, p. 308.

2. Hagenbook, L.D., and Holstein, J.H., "Universal
    Joints", Product Engineering, Vol. 13, No. 6,
    1942, pp. 334-336.

3. Rosenberg, R.M., "On the Dynamical Behavior of
    Rotating Shafts Driven by Universal (Hooke)
    Coupling", Journal of Applied Mechanics, March
    1958 , pp. 47-51.

4. Volterra, E., and Zachmanoglou, E.C., "Dynamics
    of Vibrations", Charles E. Merrill Books, Inc.,
    Columbus, Ohio, 1965, pp. 299-301.

5. Conte, S.D., "Elementary Numerical Analysis", McGraw-
    Hill Book Company, Inc., New York, 1965, pp. 220-225.

6. "System/360 Scientific Subroutine Package (360A-
    CM-03X) Version III", IBM Corporation, New York,
    1968, pp. 333-336.

CHAPTER VIII

VITA

Narayandas Trikamdas Ashar was born on August 4, 1942 in Pandharpur, India. He received his primary and secondary education in Bombay, India. He received a Bachelor of Engineering degree in Electrical Engineering in June 1964 and a Bachelor of Engineering degree in Mechanical Engineering in June 1965 from the University of Bombay, India.

He worked for six months as a Trainee Engineer in Emkay Engineering Works, Bombay and thereafter as an Assistant Engineer in Gansons Private Limited, Bombay from April 1966 to December 1968.

He has been enrolled in the Graduate School of the University of Missouri-Rolla since January 1969.